Received: 30 January 2018 | Accepted: 29 August 2018

DOI: 10.1111/jmg.12449

ORIGINAL ARTICLE

WILEY Journal of METAMORPHIC GEOLOGY

Contrasting degrees of recrystallization of carbonaceous material in the Nelson aureole, British Columbia and Ballachulish aureole, Scotland, with implications for thermometry based on Raman spectroscopy of carbonaceous material

Oliver Beyssac[1] | **David R. M. Pattison**[2] | **Franck Bourdelle**[3]

[1]IMPMC, UMR 7590, Sorbonne Université-CNRS-MNHN-IRD, Paris, France

[2]Department of Geoscience, University of Calgary, Calgary, AB, Canada, T2N 1N4

[3]LGCgE, Cité Scientifique, Université de Lille, Villeneuve d'Ascq, France

Correspondence
Oliver Beyssac, IMPMC, UMR 7590, Sorbonne Université-CNRS-MNHN-IRD, Case Courrier 115, 4, place Jussieu, 75005 Paris, France.
Email: olivier.beyssac@upmc.fr

Funding information
Natural Sciences and Engineering Research Council of Canada, Grant/Award Number: 037233; City of Paris; Sorbonne Université

Handling Editor: Doug Robinson

Abstract

The degree of recrystallization of carbonaceous material (CM), as monitored by Raman microspectroscopy, was examined as a function of metamorphic grade in two well-studied contact aureoles containing carbonaceous pelites: the Nelson aureole, British Columbia and the Ballachulish aureole, Scotland. Here, we use (a) the R2 ratio extracted from the Raman spectrum of CM as a proxy for the degree of graphitization (0.0 in perfect graphite then increasing with structural defects) and (b) the second-order S1 band (~2,700 cm^{-1}) as a marker for the tridimensional ordering of CM. The Nelson aureole (garnet–staurolite–andalusite–sillimanite–K-feldspar sequence, ~550–650°C, 3.5–4.0 kbar) was developed in rocks that were unmetamorphosed prior to contact metamorphism, whereas the Ballachulish aureole (cordierite–andalusite–K-feldspar–sillimanite sequence, ~550–700°C, ~3.0 kbar) was developed in rocks that had been metamorphosed to garnet grade conditions (~7 kbar, ~500°C) *c.* 45 Ma before contact metamorphism. Thirty-one samples were examined from Nelson and 29 samples from Ballachulish. At Nelson, the R2 ratio steadily decreases from ~0.25 to 0.0 as the igneous contact is approached, whereas at Ballachulish, the R2 ratio remains largely unchanged from regional values (~0.20–0.25) until less than 100 m from the igneous contact. The second-order S1 band reveals that carbonaceous material (CM) was transformed to highly "ordered" locally tridimensional graphitic carbon at Ballachulish by regional metamorphism prior to contact metamorphism, whereas CM was still a disordered turbostratic (bidimensional) material before contact metamorphism in the case of Nelson. Pretexturation of CM likely induced sluggish recrystallization of CM and delayed graphitization in the Ballachulish aureole. Temperatures of recrystallization of the CM in the two aureoles were estimated using different published calibrations of the thermometry based on Raman Spectroscopy of Carbonaceous Material (RSCM), with differences among the calibrations being minor. In the Nelson aureole, temperatures are in reasonable agreement with those indicated by the metapelitic phase equilibria (all within 50°C, most within 25°C). In the Ballachulish aureole, the retarded crystallization noted above results in increasing underestimates of temperatures compared to the metapelitic phase equilibria (up to ~75°C too low within 200 m of the igneous

contact). Our study calls for careful attention when using RSCM thermometry in complexly polymetamorphosed rocks to assess properly the meaning of the calculated temperature.

1 | INTRODUCTION

Carbonaceous material is widespread in metasedimentary rocks and derives from the transformation during burial of organic matter initially trapped in sediments. In such rocks, conversion of CM (here used to describe any organic compound present in rocks) into graphite (here used to describe the crystalline form of carbon) during graphitization has been studied in many geological settings. Techniques used to investigate the graphitization process include electron microscopy, Raman spectroscopy and X-ray diffraction (see Buseck & Beyssac, 2014 and references therein, for a review). In the laboratory, graphitization is a process influenced by many parameters like temperature (*T*), pressure (*P*), time or fluid activity as shown by experiments (Beyssac, Brunet, Petitet, Goffé, & Rouzaud, 2003; Nakamura, Yoshino, & Satish-Kumar, 2017). However, on geological time-scales, the degree of graphitization, a term here used to describe the bulk physico-chemical structure of CM, is considered as a proxy for the thermal metamorphism affecting either terrestrial rocks (Wopenka & Pasteris, 1993) or meteorites (e.g., Busemann, Alexander, & Nittler, 2007). The degree of graphitization in metamorphic rocks is best characterized by Raman microspectroscopy because it is highly sensitive to the physico-chemical transformation of CMs (e.g., Beyssac & Lazzeri, 2012), and can be easily conducted using petrological thin sections (polished and uncovered).

Quantitative thermometry based on Raman Spectroscopy of Carbonaceous Material (here termed RSCM thermometry) has been established by comparing the degree of graphitization as quantified by Raman spectroscopy with temperature estimates from conventional petrology (Beyssac, Goffé, Chopin, & Rouzaud, 2002). This initial calibration of the RSCM thermometer was developed for regional metamorphic rocks having undergone a single metamorphic event, and was later tested for contact metamorphism affecting aureoles in the vicinity of granitic intrusions (Aoya et al., 2010). The results from regional and contact metamorphism which have very different time-scales of heating, suggest that time is not a controlling factor for graphitization in most metamorphic settings (Aoya et al., 2010; Hilchie & Jamieson, 2014). This is in agreement with recent kinetic modelling of graphitization which shows that this transformation proceeds rapidly during metamorphism (Nakamura et al., 2017). In addition, owing to the irreversible character of the graphitization "process" and in agreement with the fact that graphite is the thermodynamically stable phase for most *P–T* conditions recorded by exhumed metamorphic rocks, RSCM thermometry indicates the peak temperature during a metamorphic cycle as CM is not affected by retrogression (Beyssac, Goffé, et al., 2002). The RSCM thermometer is especially useful in low-grade rocks in which silicate and carbonate minerals are fine grained and provide ambiguous or poorly constrained temperature estimates, and in higher grade rocks that contain nondiagnostic mineral assemblages due to a limiting chemistry of the host rock. One unknown question is the degree to which CM recrystallizes during metamorphism if it has already been subjected to an earlier episode of metamorphism. Because the degree of recrystallization is irreversible, little if any recrystallization is expected if the temperature of the later metamorphism is lower than that of the earlier metamorphism. For the reverse situation, the question is whether recrystallization proceeds continuously once the temperature of the later metamorphism exceeds that of the earlier metamorphism.

To address this question and investigate its implications for RSCM thermometry, the degree of graphitization was examined in two well-studied contact aureoles: the Nelson aureole in southeastern British Columbia, Canada (Pattison & Vogl, 2005), and the Ballachulish aureole in the southwest Highlands of Scotland (Pattison & Harte, 1997, and references therein). Figures 1 and 2 show maps of the Nelson and Ballachulish aureoles respectively. The host rocks to the Nelson aureole are essentially unmetamorphosed, subgreenschist facies carbonaceous argillites, whereas the host rocks to the Ballachulish aureole are graphitic slates that had previously been regionally metamorphosed to Barrovian garnet zone (lower amphibolite facies) conditions *c.* 45 Ma prior to intrusion and contact metamorphism (Pattison, 2013). The part of the Nelson aureole examined in this study is the same as that analysed by Pattison and Tinkham (2009) in their study of equilibrium and kinetic controls on mineral assemblage development in contact metamorphism. In this transect, the mineral assemblage sequence is garnet–staurolite–andalusite–sillimanite–K-feldspar, indicating a pressure of 3.5–4.0 kbar and a temperature range of ~550°C to ~650°C. The part of the Ballachulish aureole examined in this study is the same as that analysed by Pattison (2006)

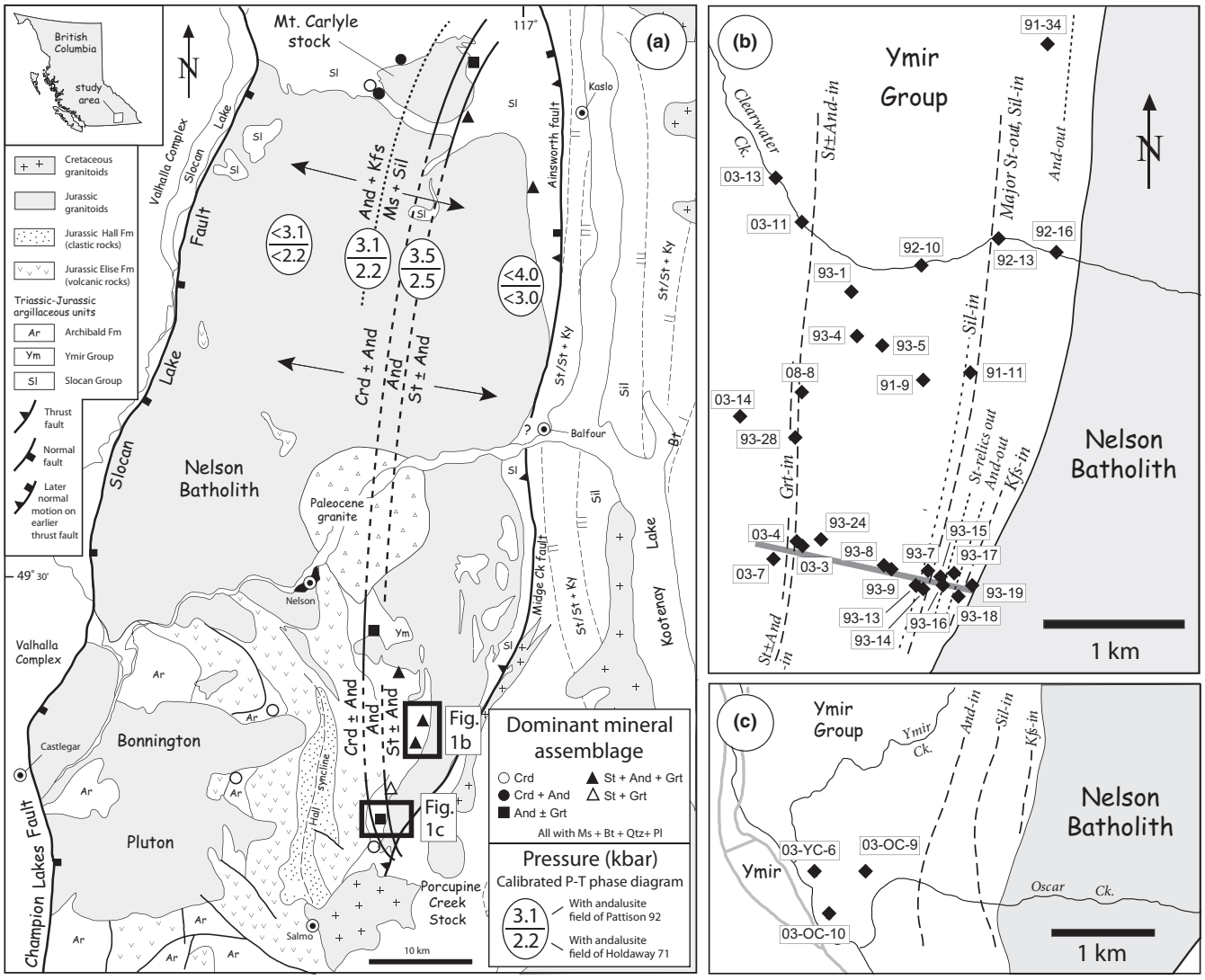

FIGURE 1 (a) Regional map of the Nelson batholith and aureole, adapted from Pattison and Vogl (2005) and Moynihan and Pattison (2013). Dashed lines separate mineral assemblage domains of different pressure, that is, they are not isograds (see Pattison & Vogl, 2005, for details). Metamorphic zones involving staurolite and kyanite are part of a regional Barrovian metamorphic culmination that occurs east of the major Gallagher–Midge Creek fault zone, and which is unrelated to the metamorphism in the study area. (b) Isograds and sample locations (Table 2) from the main study area, adapted from Pattison and Tinkham (2009). Isograds marking the first appearance of index minerals are shown in long dashed lines and those showing the disappearance of index minerals are shown in short dashed lines. The grey solid line is the line used for measuring distances of samples from the contact (see text for discussion). (c) Location of samples from south of the main study area

in his study of the variation in abundance and textures of CM going upgrade in the aureole. In this transect, the mineral assemblage sequence is cordierite–andalusite–sillimanite–K-feldspar–migmatite, indicating a pressure of 2.5–3.0 kbar and a temperature range of ~550 to ~700°C. In the present study, 31 samples from Nelson and 29 samples from Ballachulish were analysed by RSCM and combined with observations on the microtextural evolution of the CM in the aureoles. Results from the two aureoles are synthesized, and then implications for RSCM thermometry are discussed based on these results and existing literature.

2 | RSCM THERMOMETRY AND METHODOLOGY

2.1 | Graphitization in metamorphism and RSCM thermometry

During diagenesis and metamorphism, CM present in the initial sedimentary rock is progressively transformed into graphite (see Buseck & Beyssac, 2014 for a review). During burial in sedimentary basins, the thermally induced maturation or "cracking" of organic matter generates hydrocarbons, oil then gas, and leaves a solid residue called

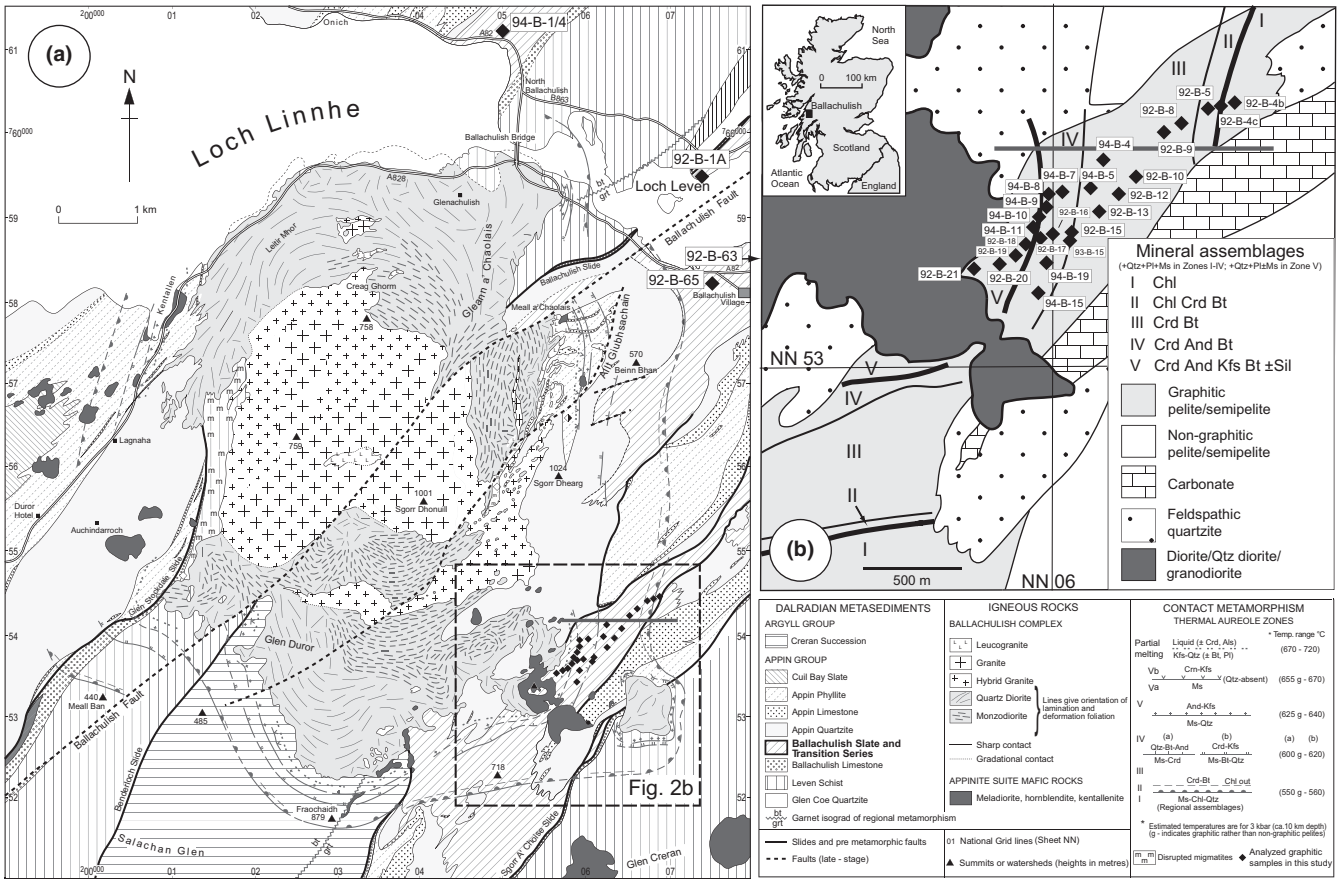

FIGURE 2 (a) Geology of the Ballachulish area, modified from fig. 7 of Pattison and Harte (2001), itself based on Weiss and Troll (1989) and Pattison and Harte (1997). The grey solid line is the line of section, approximately normal to the igneous contact, into which sample distances were projected (see text). (b) Metamorphic zones, isograds, and sample locations (Table 3) in the area of interest. The grey solid line is the line of section, approximately normal to the igneous contact, into which sample distances were projected (see text)

kerogen. This solid residue is carbon rich as most heteroatoms (H, O, N, S) have been released, and it has initiated the development of an aromatic skeleton consisting of a network of six-membered, planar rings of carbon. This solid residue, if subjected to further heating during metamorphism, will be subject to graphitization *sensu stricto*, which consists mostly in the polymerization and structural rearrangement of the aromatic skeleton towards the thermodynamically stable ABAB-layered sequence of graphite. The corresponding progressive evolution of the degree of graphitization is considered to be a reliable indicator of metamorphic temperature (Beyssac, Goffé, et al., 2002; Wopenka & Pasteris, 1993). Because of the irreversible character of graphitization (CM tends towards the thermodynamically stable phase which is graphite), CM structure is not sensitive to the retrograde path of the rock up to the surface, and therefore records peak metamorphic conditions (Beyssac, Goffé, et al., 2002).

Raman microspectroscopy is ideally suited to the study of natural CM in situ within uncovered, polished thin sections. The first-order Raman spectrum of disordered CM exhibits a graphite G band at 1,580 cm^{-1}, E_{2g2} mode corresponding to in-plane vibration of aromatic carbons, and several defect bands (D1, D2, D3) corresponding to "physico-chemical defects" (see Beyssac & Lazzeri, 2012 and references therein). The structural organization of CM can be quantified through the R2 parameter, defined as the relative area of the main defect band D1 (R2=D1/[G+D1+D2] peak area ratio). A linear correlation between this R2 parameter and metamorphic temperature was calibrated using samples from different regional metamorphic belts with well-known *P–T* conditions spanning a temperature range of 330–640°C, giving rise to RSCM thermometry (Beyssac, Goffé, et al., 2002). RSCM thermometry can be applied to metasedimentary rocks of various lithologies. The uncertainty on temperature is ±50°C mainly due to uncertainties on petrological data used for the calibration. However, Beyssac, Bollinger, Avouac, and Goffé (2004) showed that this technique might be used to detect inter-sample relative variations as small as 10–15°C, allowing for a precise estimate of thermal metamorphic gradients. CM exhibits second-order features in the Raman spectrum

corresponding to combination and overtone scattering (see Beyssac & Lazzeri, 2012 for review). The second-order region provides information on the tridimensional stacking order of graphitic CM. When turbostratic (imperfect stacking of the aromatic layers yielding bidimensional stacking) graphitic carbon reaches the three-dimensional structure of graphite (ABAB stacking sequence), the main second-order band at ~2,700 cm^{-1}, corresponding to a multiple of the D1 band and here called the S1 band becomes asymmetric and can be decomposed into two bands centred at ~2,690 and 2,730 cm^{-1} respectively (see Bernard et al., 2010; Beyssac & Lazzeri, 2012; Lespade, Marchand, Couzi, & Cruege, 1984).

2.2 | Raman spectroscopy: Methodology

Raman spectra were obtained at Institut de Minéralogie, Physique des Matériaux et Cosmochimie (Paris, France) using a Renishaw InVia Raman microspectrometer. The 514.5-nm wavelength of a Modulaser argon laser was used. The laser incident beam was polarized circularly by a quarter wavelength plate placed before the microscope. The laser was focused on the sample by a DMLM Leica microscope with a 100 magnification objective (numerical aperture = 0.85) and the spot size at the sample surface is ~1 μm in diameter. The laser power at the sample surface was set below 1 mW using neutral density filters. The Rayleigh diffusion was eliminated by notch filters and the signal was finally dispersed using a 1,800 gr/mm grating and analysed by a Peltier cooled RenCam CCD detector. Before each session the spectrometer was calibrated with a silicon standard.

Because Raman spectroscopy of CM can be affected by several analytical mismatches, we followed closely the analytical and fitting procedures described by Beyssac, Goffé, et al. (2003) and Beyssac and Lazzeri (2012). Measurements were done on polished thin sections cut perpendicularly to the bedding and/or schistosity. CM, being black, has a very high extinction coefficient for visible light and therefore Raman spectroscopy only probes a thin (100s of nm thick) surface layer of CM, which makes this technique highly sensitive to the surface state of the sample. As RSCM is controlled by defects in CM, it is important to avoid any possible sample preparation bias such as structural defects induced by polishing. Therefore, CM was systematically analysed below a transparent adjacent mineral, generally quartz, to avoid any polishing-induced artefact on the structure of CM. In metamorphic settings, especially in the case of contact metamorphic settings where CM can exhibit high degrees of graphitization and very fine-grained microtextures, polished petrological thin sections must be used rather than polished rock chips. Using polished thin sections is the only way to use both transmitted and reflected light to make sure that the CM target is at depth and not at the sample surface.

To gain insight on the within-sample structural heterogeneity, at least 15–20 Raman spectra were recorded per sample. However, some samples exhibited a rather high structural heterogeneity and required acquisition of more spectra. Importantly, detrital graphitic carbon was found locally in both of the aureoles examined. The presence of detrital graphite is common because graphite is easily recycled during the erosion/weathering cycle (see Galy, Beyssac, France-Lanord, & Eglinton, 2008). It can be easily distinguished from organic matter that is undergoing in situ graphitization based on: (a) morphological criteria—it generally appears as isolated grains or flakes, and (b) Raman spectra—it usually exhibits a high crystallinity except in very high-grade samples where it is difficult to distinguish from the metamorphosed organic matter based on Raman spectroscopy alone. Detrital graphite spectra were not included in RSCM temperature determination. Spectra were then processed using the software Peakfit following the procedure described in Beyssac, Goffé, et al. (2003) and Beyssac and Lazzeri (2012).

3 | THERMODYNAMIC MODELLING

The *P–T* estimates of isograds in the Nelson aureole were made by Pattison and Tinkham (2009), and in the Ballachulish aureole by Pattison (1989, 2006). These estimates were based on phase equilibria modelling that used different thermodynamic data sets and, in the case of Nelson, did not incorporate the effects of graphite. In this study, we have recalculated the phase equilibria using a single set of thermodynamic data and mineral activity–composition (*a–x*) models and have incorporated the effects of graphite.

For Nelson, the bulk composition used for the modelling is the average Nelson carbonaceous argillite composition (pp. 71–72 of Pattison & Vogl, 2005 and table 1 of Pattison & Tinkham, 2009), whereas for Ballachulish, the bulk composition is the average composition of the carbonaceous slates of Ballachulish Slate (table 1 and appendix 2 of Pattison, 2013). Both compositions are listed in Table 1 of this paper. The thermodynamic modelling was done in the model chemical system MnNCKFMASHT ($MnO–Na_2O–CaO–K_2O–FeO–MgO–Al_2O_3–SiO_2–H_2O–TiO_2$), in which C, P_2O_5, and LOI (loss on ignition) were omitted from the raw whole-rock analysis. All Fe was treated as Fe^{2+}, in respect of the relatively reducing nature of the carbonaceous rocks. All mineral assemblages examined in this study developed under subsolidus conditions, so excess H_2O was assumed. The presence of graphite in the rocks results in small concentrations of carbon-bearing fluid species in the metamorphic fluid, lowering a_{H2O}. This effect

TABLE 1 Whole-rock compositions used for thermodynamic modelling

wt%	Nelson Average Ymir argillite[a]	Ballachulish Average Ball. Slate[b]
SiO_2	60.41	60.68
TiO_2	0.93	0.84
Al_2O_3	20.10	19.94
FeO	5.68	5.20
MnO	0.08	0.05
MgO	2.30	3.44
CaO	1.06	0.12
Na_2O	1.53	1.50
K_2O	4.17	3.80
P_2O_5	0.15	0.07
LOI	3.09	3.82
Total	99.51	99.46
S	0.03	0.17
C	0.31	0.65
Moles elements × 100; MnNCKFMASHT (C and P dropped; projected from pyrrhotite)		
Si	100.55	100.98
Ti	1.17	1.05
Al	39.43	39.12
Fe	7.82	6.71
Mn	0.12	0.07
Mg	5.70	8.54
Ca	1.90	0.22
Na	4.92	4.84
K	8.85	8.07
Mg#	0.419	0.541
Mg# (S)	0.422	0.560
Mg#(S+Ti)	0.462	0.560
A′	0.144	0.240
Mn#	0.008	0.004
Ca#	0.122	0.013

Mg#=Mg/(Mg+Fe).
Mg#(S)=Mg/(Mg+Fe), after projection from pyrrhotite.
Mg#(S+Ti)=Mg/(Mg+Fe), after projection from pyrrhotite and ilmenite (not for rutile-bearing Ballachulish Slate).
A′=(Al–Na–2Ca–3K)/2.
Mn#=Mn/(Mn+Fe+Mg+Ca).
Ca#=Ca/(Mn+Fe+Mg+Ca).
[a]Raw analysis from table 1 of Pattison and Tinkham (2009). [b]Raw analysis from appendix 2 of Pattison (2013).

was incorporated into the phase equilibria modelling following the approach of Connolly and Cesare (1993).

The phase diagrams were calculated using the phase equilibria modelling software program Theriak-Domino (De Capitani & Brown, 1987; De Capitani & Petrakakis, 2010). The thermodynamic data set used to calculate the phase diagrams is that of Holland and Powell (1998), updated to version ds5.5. The *a–x* relations used in conjunction with ds5.5 comprise the following: garnet and chlorite, Tinkham, Zuluaga, and Stowell (2001); biotite, White, Pomroy, and Powell (2005); plagioclase, Holland and Powell (2003; ternary feldspar, Cbar1 field); white mica, Coggon and Holland (2002; margarite component omitted); ilmenite, Tinkham and Ghent (2005; ideal ternary); melt, White, Powell, and Holland (2007); all other phases including H_2O, Holland and Powell (1998). Use of the 2007 "Thermocalc331" *a–x* relations (http://www.metamorph.geo.uni-mainz.de/thermocalc/software/index.html) with data set ds5.5, or use of the Holland and Powell (2011) data set ds6.2 with the *a–x* models of White, Powell, Holland, Johnson, and Green (2014), White, Powell, and Johnson (2014), result in poorer models of low-*P* subsolidus metapelitic phase equilibria, as discussed in Pattison and DeBuhr (2015). Even with the preferred data set and *a–x* models, some aspects of the modelled phase equilibria do not match the natural constraints (discussed in more detail below), but these disparities do not compromise the key temperature constraints in the two aureoles.

4 | GEOLOGICAL BACKGROUND

4.1 | The Nelson Batholith and aureole

4.1.1 | Local geology

The Nelson Batholith (Figure 1a) is one of the largest of a suite of middle Jurassic plutons, known as the Nelson suite, in southeastern British Columbia (e.g., Archibald, Glover, Price, Carmichael, & Farrar, 1983). The batholith is emplaced in Triassic–Jurassic carbonaceous argillaceous rocks of the Ymir and Slocan groups that were essentially unmetamorphosed (subgreenschist facies) prior to intrusion of the Nelson suite (Morgan, 2016; Powell & Ghent, 1996; Starr, 2017). The composite batholith ranges from tonalite to granite and comprises a northern mass, including the Mt. Carlyle Stock, of ~30 × 50 km^2 (referred to as the main body) and a 25-km-long southern "tail" (Little, 1960; Vogl & Simony, 1992) (Figure 1a). U–Pb dating indicates that the different phases of the batholith were intruded in the Jurassic between *c.* 173 and 159 Ma (Ghosh, 1995; Parrish, 1992; Sevigny & Parrish, 1993). Geophysical and petrological data suggest that the northern mass of the batholith is a tabular, flat-bottomed body, 2–7 km below present-day sea level (Cook et al., 1988), whereas the southern "tail" of the batholith, which is the focus of this

study, shows subvertical contacts with the host rocks (Vogl & Simony, 1992).

A 0.7–1.8-km-wide contact aureole surrounds the batholith, based on the outermost development of porphyroblasts of cordierite, staurolite or andalusite. U–Pb dating of monazite produced during contact metamorphism is the same age, within error, as the intrusion (Tomkins & Pattison, 2007). As shown in Figure 1a, higher pressure staurolite±andalusite-bearing mineral assemblage sequences are restricted to the aureole surrounding the east half of the batholith, whereas lower pressure cordierite±andalusite-bearing mineral assemblage sequences are restricted to the aureole surrounding the west half of the batholith and its northern and southern tips (Pattison & Vogl, 2005). These data indicate that the batholith and aureole are tilted ~10° to the west, with the tilting ascribed to a combination of Jurassic–Cretaceous contractional deformation and Eocene extension (Pattison & Vogl, 2005). Figure 1b,c shows the part of the aureole examined in this study, with Figure 1b corresponding to Area D of Pattison and Vogl (2005). Area D was studied in further detail by Pattison and Tinkham (2009), and the isograds in Figure 1b come from this latter study.

4.1.2 | Isograds

The sequence of mineral-in isograds in the study area is garnet, staurolite±andalusite, sillimanite, and K-feldspar (Figure 1b). The garnet and staurolite±andalusite isograds are nearly coincident. The above prograde sequence classifies as facies series 2b (staurolite–andalusite) in the scheme of Pattison and Tracy (1991).

Two major dehydration intervals in the isograd sequence correspond to the consumption of chlorite and muscovite respectively. The first interval, involving chlorite consumption, is associated with the closely spaced garnet, staurolite and andalusite isograds, ~1,400 m from the contact. The idealized reactions introducing these porphyroblasts, written in the model KFMASH chemical system, are, respectively, (abbreviations of Kretz, 1983):

$$\mathrm{Ms+Chl+Qtz = Grt+Bt+H_2O} \quad \text{(N1)}$$

$$\mathrm{Ms+Grt+Chl+Qtz = St+Bt+H_2O} \quad \text{(N2)}$$

$$\mathrm{Ms+St+Chl = And+Grt+Bt+Qtz+H_2O} \quad \text{(N3)}$$

$$\mathrm{Ms+St+Qtz = And+Grt+Bt+H_2O} \quad \text{(N4)}$$

(The prefix "N" in the reaction numbering is used to distinguish numbered reactions in the Nelson aureole from those in the Ballachulish aureole). However, the lack of textural evidence for the participation of garnet in reaction N2 and of staurolite in reactions N3 and N4 (i.e., lack of evidence for dissolution) in the vicinity of the isograds suggests that all three porphyroblasts developed from the reaction of matrix minerals (Pattison & Tinkham, 2009). The reactions producing staurolite and andalusite were therefore interpreted to be:

$$\mathrm{Ms+Chl+Qtz = St+Bt+H_2O} \quad \text{(N5)}$$

$$\mathrm{Ms+Chl = And+Bt+Qtz+H_2O} \quad \text{(N6)}$$

Pattison and Tinkham (2009) ascribed the clustering of the garnet, staurolite and andalusite isograds to a "cascade effect" triggered by the overstepped, kinetically delayed nucleation and growth of garnet, and concomitant release of fluid.

The second major dehydration reaction in the aureole is associated with the development of coexisting sillimanite and K-feldspar and the loss of primary (foliation-defining, as opposed to alteration-related) muscovite:

$$\mathrm{Ms+Qtz = Sil+Kfs+H_2O.} \quad \text{(N7)}$$

In some samples, K-feldspar occurs in medium coarse-grained leucosomes (fig. 6g of Pattison & Vogl, 2005), suggesting that reaction N7 locally may have been a partial melting reaction such as:

$$\mathrm{Ms+Pl+Qtz = Sil+Kfs+melt.} \quad \text{(N8)}$$

Between these two major dehydration intervals are a number of other isograds. The sillimanite isograd occurs ~400 m from the intrusive contact and is marked by small amounts (≪1 modal %) of fibrolitic and fine-grained sillimanite that occurs in the matrix and on the margins of andalusite and staurolite porphyroblasts. Three hundred metres from the contact, staurolite decreases markedly and sillimanite increases markedly, shown in Figure 1b as the "major staurolite-out, sillimanite-in" isograd. Combined with evidence for a second generation of garnet growth, this latter change is ascribed to the reaction:

$$\mathrm{Ms+St+Qtz = Sil+Grt+Bt+H_2O.} \quad \text{(N9)}$$

The delayed progress of the staurolite-consuming reaction in most of the rocks, producing sillimanite (reaction N9) rather than andalusite (reaction N4), was ascribed to the small free energy change in the reaction and a change in the nucleation kinetics arising from the development of sillimanite (Pattison & Tinkham, 2009, p. 276).

4.1.3 | Pressure of contact metamorphism and isograd temperatures

Figure 3a shows a phase diagram calculated for the average Nelson carbonaceous argillite. The isograd sequence in the

aureole (garnet; staurolite±andalusite; sillimanite; K-feldspar) is possible within the range 3.3–4.0 kbar. The clustered staurolite-in and andalusite-in isograds favour a pressure at the lower end of this range, ~3.5 kbar (see also Pattison & Tinkham, 2009).

The temperatures of the isograds in the Nelson aureole are based on the 3.5-kbar isobaric transect through the phase diagram in Figure 3a. They are 3–8°C lower than those in table 2 of Pattison and Tinkham (2009), due to lowered a_{H2O} in the hydrous fluid phase because of CM in the rocks, a factor that was not taken into account in the earlier study.

The two reaction isograds that anchor the temperature profile in the Nelson aureole are the chlorite-consuming, staurolite/andalusite-producing reaction isograd and muscovite-consuming, sillimanite+K-feldspar-producing reaction isograd. Concerning the chlorite-consuming reactions, the staurolite- or andalusite-producing reactions (reactions N2–N6), whether stable or metastable, cluster in a small, <10°C interval, centred on 555°C, shown as an open circle in Figure 3a. Because they are all high-entropy reactions, they will be least affected by any possible overstepping (Pattison, de Capitani, & Gaidies, 2011). Over the pressure range of contact metamorphism of 3.3–4.0 kbar (Pattison & Tinkham, 2009), reactions N2–N6 occur in the range 550–570°C. Incorporating some further uncertainty arising from uncertainty in the thermodynamic data, the preferred estimate for the chlorite-consuming, garnet/staurolite/andalusite-producing reaction isograd is 555 ± 20°C. For the muscovite-consuming reaction isograd (reaction N7), the estimated temperature at 3.5 kbar is 645°C (open circle in Figure 3a). Over the pressure range of 3.3–4.0 kbar, the temperature range is 640–660°C (Figure 3a), which combined with some thermodynamic uncertainty results in an estimate of 645 ± 20°C for this reaction isograd.

The other isograd reactions in the aureole do not provide robust constraints on temperature. As noted above, the staurolite-consuming reaction (reactions N4 and N9) has been significantly overstepped, and the nature of the reaction introducing sparse sillimanite is obscure (Pattison & Tinkham, 2009).

The temperature estimates of the chlorite-consuming and muscovite-consuming reaction isograds are combined with the distance of the isograds from the contact (Figure 1b,c) to produce a temperature versus distance profile in Figure 4a. Temperature estimates of samples between and outside (at lower grade than) the two anchoring reaction isograds (filled circles in Figure 3a) are interpolated by eye, guided by the gently curving shape of the temperature-distance profile in fig. 14 of Pattison and Tinkham (2009), and thus are not independent estimates. For samples between the isograds, the added temperature uncertainty arising from this

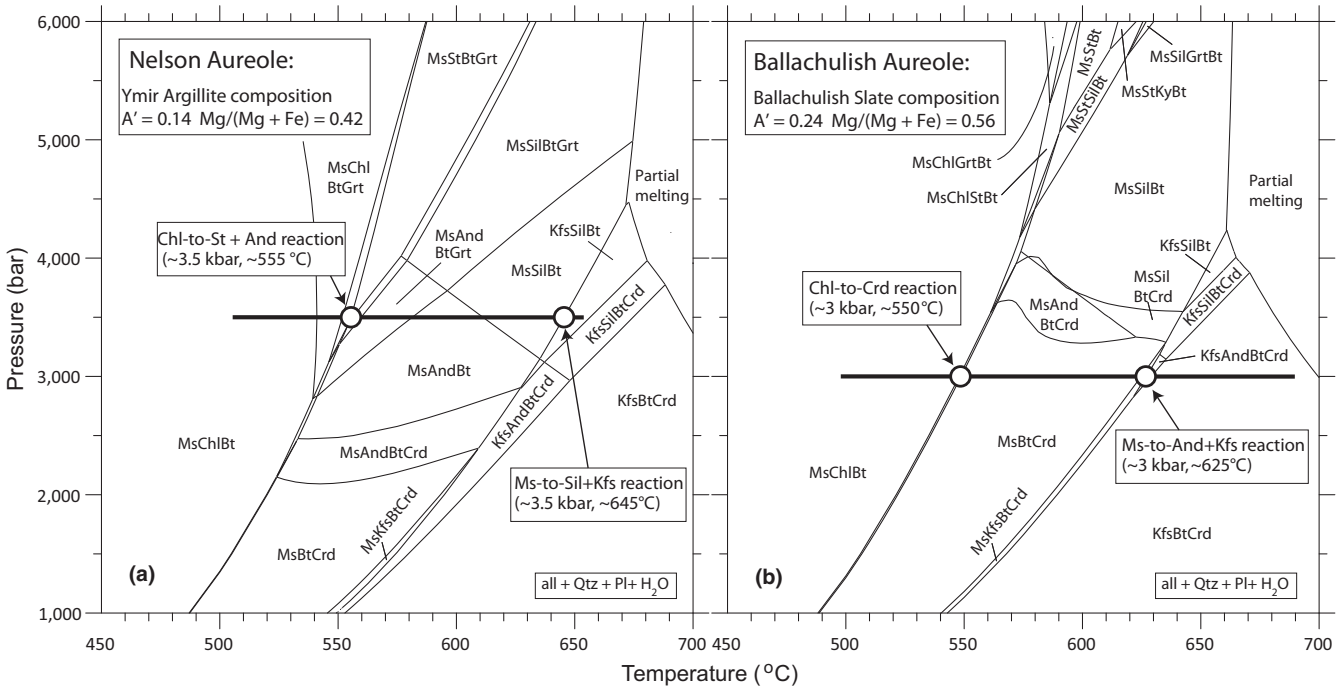

FIGURE 3 (a) Thermodynamically calculated phase diagram for the average carbonaceous argillite (Ymir argillite) from the Nelson aureole (composition listed in Table 1, where aluminium index, A′, is defined). See text for details of phase diagram calculation. Solid isobaric line and two identified reaction intervals discussed are discussed in text. Andalusite–sillimanite boundary from Pattison (1992). (b) Thermodynamically calculated phase diagram for the average carbonaceous slate (Ballachulish Slate) from the Nelson aureole (composition listed in Table 1). Solid isobaric line and two identified reaction intervals discussed are discussed in text

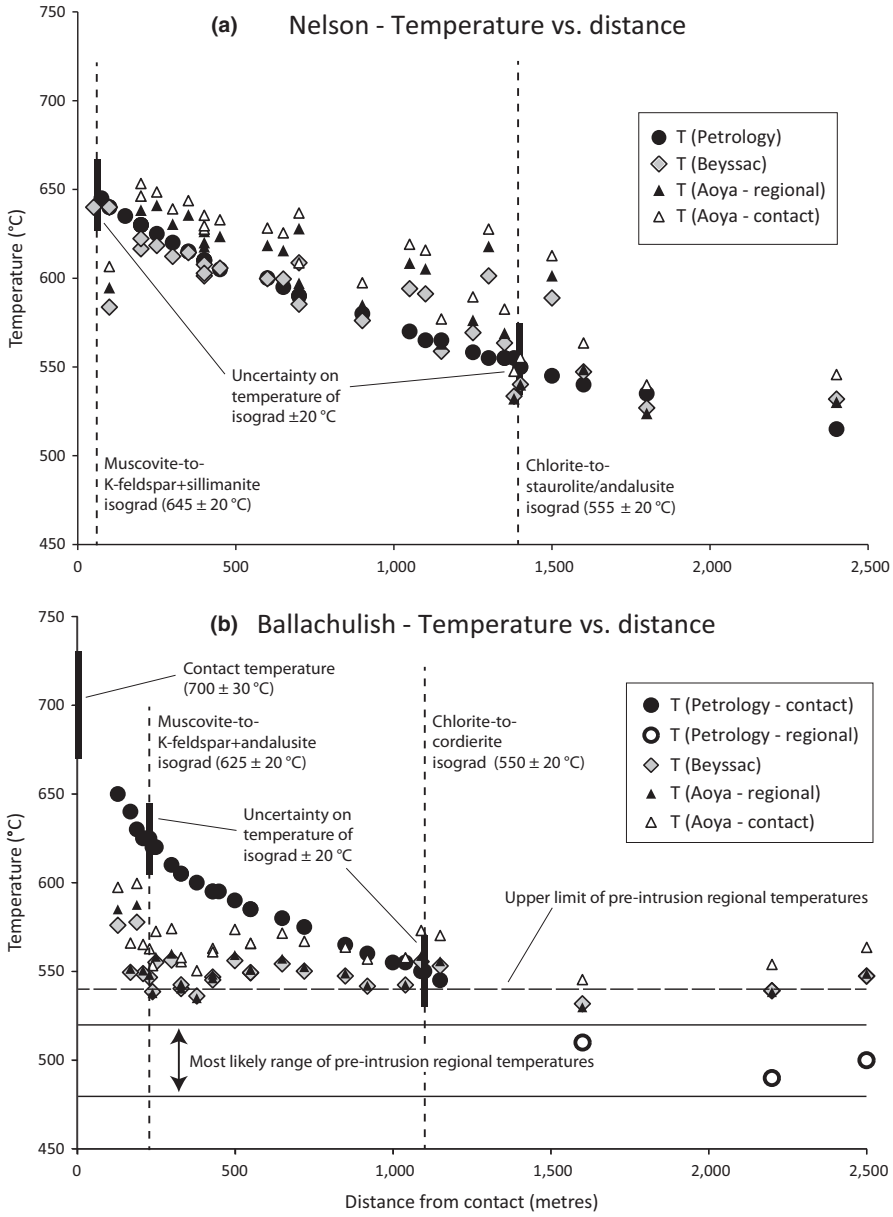

FIGURE 4 (a) Temperature estimates versus distance from contact in the Nelson aureole, based on data in Table 2. Sample locations and isograd locations from Figure 1b,c. Uncertainities on temperature estimates from petrology: ±20°C (see text for discussion). Uncertainities on temperature estimates from graphite thermometry: ±50°C (see text for discussion). (b) Temperature estimates versus distance from contact in the Ballachulish aureole, based on data in Table 3. Sample locations and isograd locations from Figure 2a,b. Uncertainities on temperature estimates of aureole rocks as above. See text for discussion of temperature estimates and uncertainties for the regional rocks at Ballachulish

interpolation method will be small, probably <±10°C, whereas for samples at the greatest distance from the intrusive contacts, outside the chlorite-consuming reaction isograd, uncertainty arising from interpolation could increase to ±15–20°C. Distances in Figure 4a and Table 2 are based on the grey section line shown in Figure 1b, with samples away from the transect interpolated into the line of section based on their position relative to the isograds, yielding uncertainties of ±30 m. Samples from Figure 1c have a larger uncertainty (±200 m).

4.1.4 | Temperature of host rocks outside the aureole

Temperature estimates for the regional rocks at the time of intrusion are not well constrained. Powell and Ghent (1996), Morgan (2016), and Starr (2017) mapped a series of regional isograds in the area demonstrating an increase in metamorphic grade as the plutons of the Nelson suite were approached, from prehnite–pumpellyite (subgreenschist) facies to lower amphibolite facies close to the intrusive contacts. One of the isograds they mapped was a biotite-in isograd in carbonaceous argillites. The lowest grade argillaceous rocks sampled in this study (Figure 1c) come from the biotite zone, that is, upgrade of this biotite isograd. Petrographic observation of these rocks shows that the biotite occurs as small crystals at random orientations in the matrix, similar to the grain size and texture of biotite in samples from the narrow garnet zone of the aureole. We therefore interpret that the biotite in these low-grade samples developed as part of the contact metamorphism associated with the Nelson intrusion, rather than being part of a

separate, preintrusion, regional metamorphic biotite zone as suggested in Pattison and Vogl (2005) and Pattison and Tinkham (2009). The method of estimating temperatures of biotite-bearing samples outward from (at a lower grade than) the clustered garnet/staurolite/andalusite isograds in Figure 1b,c is discussed above in Section 4.1.3.

4.2 | The Ballachulish intrusive complex and aureole

4.2.1 | Local geology

The second locality chosen is the aureole surrounding the Ballachulish Igneous Complex, Scotland (Pattison & Harte, 1997; Voll, Töpel, Pattison, & Seifert, 1991), illustrated in Figure 2a. The 425 ± 4 Ma igneous complex (Fraser, Pattison, & Heaman, 2004) was emplaced in metasedimentary rocks belonging to the Dalradian Supergroup (Pattison & Voll, 1991). Prior to emplacement of the igneous complex, the host metasedimentary rocks were subjected to two phases of penetrative deformation and were metamorphosed to Barrovian garnet zone conditions (~7 kbar, ~500°C; Pattison, 2013) during regional orogenesis at *c.* 470 Ma (Grampian phase of the Caledonian orogeny).

The intrusion consists of an outer orthopyroxene-bearing diorite shell (emplaced at~1, 100°C) surrounding a central body of granite (emplaced at ~850°C), the latter emplaced when the central portion of the diorite was still partially molten (Weiss & Troll, 1989, 1991). A well-developed contact aureole surrounds the intrusive complex, ranging in width from 400 to 1,700 m, based on the outermost occurrence of cordierite "spots" (Figure 2a). Isograds in pelitic rocks, the most abundant rock type in the aureole, can be mapped around the intrusion and range from development of cordierite up to anatectic migmatization (Pattison, 1989; Pattison & Harte, 1985, 1991).

The contact metamorphism was mainly caused by intrusion of the diorite phase, with the later granite having little effect (Buntebarth, 1991). The duration of the contact metamorphic event, for temperatures above conditions of the cordierite-in reaction (~550°C), is estimated to have been *c.* 500 ka, whereas rocks in the inner aureole were hot enough to be partially molten (above ~660°C) for *c.* 270 ka (Buntebarth, 1991). With the exception of some fluid-fluxed partial melting on the west flank of the complex, fluid communication between the intrusion and aureole was generally limited (Ferry, 1996; Harte et al., 1991), with no evidence for development of a large-scale hydrothermal circulation system around the intrusion.

Carbonaceous slates and phyllites belonging to the Ballachulish Slate and Transition Series stratigraphic units (Pattison & Voll, 1991; and references therein) occur at various places in the contact aureole (Figure 2a). The focus of this study is a band of carbonaceous metapelite that can be traced continuously upgrade along strike in the southeast part of the aureole (Figure 2b). This band of rock was the subject of a study by Pattison (2006) on the abundance and textures of CM in the aureole, and a description of this transect is provided on pages 103–117 of the field guide of Pattison and Harte (2001). The pre-intrusion regional metamorphic grade is garnet zone (lower amphibolite facies), but the carbonaceous slates and phyllites themselves do not contain either garnet or biotite due to their relatively magnesian composition (Pattison, 2013).

4.2.2 | Isograds

Five mineral assemblage zones related to contact metamorphism, separated by four isograds, have been mapped in the carbonaceous metapelite (Pattison & Harte, 1985, 1991). The isograds are cordierite+biotite-in (Zone I/II isograd), chlorite-out (Zone II/III isograd), andalusite-in (Zone III/IV isograd), and K-feldspar-in (Zone IV/V) isograd (Figure 2b). Within Zone V, upgrade of the K-feldspar-in isograd, sillimanite, and anatectic migmatite are variably developed. This isograd sequence classifies as facies series 1b/1c (cordierite–andalusite) in the scheme of Pattison and Tracy (1991).

As at Nelson, the two major dehydration reaction isograds in the Ballachulish aureole correspond to the consumption of chlorite and muscovite respectively. The consumption of chlorite occurs in a narrow interval between the closely spaced Crd+Bt-in (Zone I/II) isograd and Chl-out (Zone II/III) isograd, and corresponds to the following reaction, written in the idealized KFMASH chemical system:

$$\mathrm{Ms+Chl+Qtz = Crd+Bt+H_2O} \qquad \text{(B1)}$$

(The "B" prefix in the numbered reactions refers to reactions in the Ballachulish aureole). In the field, the width of the interval between the first appearance of Crd+Bt and the last occurrence of primary chlorite (Zone II) is ~100 m (Figure 2b).

The second major reaction, associated with the loss of primary muscovite and development of coexisting andalusite and metamorphic K-feldspar (Zone IV/V isograd), is:

$$\mathrm{Ms+Qtz = And+Kfs+H_2O} \qquad \text{(B2)}$$

Sillimanite first occurs at or a little upgrade of the first development of andalusite+K-feldspar.

Between isograd reactions B1 and B2 is a less well-constrained isograd (Zone III/IV isograd) that marks the development of andalusite in some but not all rocks (Figure 2b). The Fe–Mg divariant reaction introducing andalusite to the Crd+Bt assemblage is:

$$\mathrm{Ms+Crd = And+Bt+Qtz+H_2O} \qquad \text{(B3)}$$

TABLE 2 Summary of data for the Nelson aureole. Refer to Figure 1b,c for sample locations

Sample	Distance from contact (m) ±30 (Figure 1b) ±200 (Figure 1c)	Assemblage	*T* (°C) ±20	*n*	R2 (avg)	*SD*	T_{B02} (°C)	*SD*	*SE*	T_{A10r} (°C)	*SD*	*SE*	T_{A10c} (°C)	*SD*	*SE*
		Samples from Figure 1c													
03-YC-6	3,200	Ms+Chl+Bt	495	23	0.24	0.07	533	31	7	532	38	8	547	36	8
03-OC-10	2,900	Ms+Chl+Bt	500	32	0.26	0.08	523	33	6	524	43	8	540	42	7
03-OC-9	2,400	Ms+Bt+Amph	515	33	0.25	0.06	532	26	5	530	31	5	546	30	5
		Samples from Figure 1b													
03-14	1,800	Ms+Chl?+Bt	535	27	0.26	0.04	527	17	3	524	20	4	540	20	4
03-13	1,600	Ms+Chl+Bt	540	31	0.21	0.06	547	27	5	549	34	6	563	32	6
03-7a	1,500	Ms+Bt	545	34	0.12	0.06	589	26	4	601	34	6	613	31	5
03-11	1,400	Ms+Chl?+Bt	550	29	0.23	0.06	540	25	5	540	31	6	555	29	5
	1,400	Garnet-in isograd	550												
93-28	1,380	Ms+Bt	555	45	0.24	0.06	534	25	4	532	31	5	548	29	4
	1,350	***Staurolite+andalusite-in isograd***	***555***												
08-8	1,350	Ms+Grt+Bt+St+And	555	31	0.17	0.07	563	30	5	569	37	7	583	35	6
03-4	1,300	Ms+Grt+Bt+St+And	555	34	0.09	0.05	601	24	4	618	33	6	628	30	5
03-3	1,250	Ms+Grt+Bt+St+And	560	22	0.16	0.07	569	30	6	576	40	8	589	36	8
93-24	1,150	Ms+Bt	565	28	0.18	0.06	559	28	5	563	36	7	577	34	6
93-1	1,100	Ms+Grt+Bt+St+And	565	23	0.11	0.08	591	37	8	605	49	10	616	45	9
93-4	1,050	Ms+Grt+Bt	570	22	0.11	0.06	594	29	6	609	38	8	619	35	7
93-5	900	Ms+Grt+Bt+St	580	25	0.15	0.06	576	26	5	585	35	7	597	32	6
92-10	700	Ms+Grt+Bt+St	590	26	0.12	0.07	585	29	6	597	38	8	609	35	7
93-8	700	Ms+Grt+Bt+St	590	22	0.07	0.06	609	26	6	628	35	7	637	32	6
93-9	650	Ms+Grt+Bt+St	595	29	0.09	0.06	600	26	5	616	35	6	626	31	6
91-9	600	Ms+Grt+Bt+St+And	600	22	0.09	0.06	600	26	6	619	33	7	628	30	6
93-13	450	Ms+Grt+Bt+St+And	605	23	0.08	0.05	606	22	5	624	29	6	633	26	6
93-7	400	Ms+Grt+Bt+St+And	610	22	0.07	0.05	608	22	5	626	29	6	635	26	6
	400	Fibrolite-in isograd	610												
91-11	400	Ms+Grt+Bt+St+And+Sil	610	24	0.09	0.05	601	23	5	618	31	6	628	28	6
93-14	400	Ms+Grt+Bt+St+And+Sil	610	18	0.09	0.06	603	29	7	620	38	9	630	35	8
	350	Major Staur-out, Sil-in isograd	615												
92-13	350	Ms+Grt+Bt+Sil	615	26	0.06	0.05	614	24	5	636	32	6	644	29	6
93-15	300	Ms+Bt+Sil	620	25	0.06	0.05	612	23	5	630	31	6	639	28	6
93-16	250	Ms+Grt+Bt+St+And+Sil	625	24	0.05	0.05	618	23	5	641	31	6	648	28	6
	200	Staur relics-out isograd	630												
91-34	200	Ms+Bt+Sil	630	25	0.06	0.04	617	20	4	638	27	5	646	24	5
93-17	200	Ms+Bt+Grt+And+Sil	630	28	0.04	0.04	622	17	3	646	24	4	653	21	4
	150	Andalusite-out isograd	635												
93-18	100	Ms+Bt+Grt+Sil	640	28	0.13	0.06	584	25	5	606	33	6	594	30	6

(Continues)

TABLE 2 (Continued)

Sample	Distance from contact (m) ±30 (Figure 1b) ±200 (Figure 1c)	Assemblage	*T* (°C) ±20	*n*	R2 (avg)	*SD*	T_{B02} (°C)	*SD*	*SE*	T_{A10r} (°C)	*SD*	*SE*	T_{A10c} (°C)	*SD*	*SE*
92-16	100	Ms+Bt+Sil	640		0.00		>641			676			672		
	75	***K-feldspar-in isograd***	***645***												
93-19a	50	Ms+Bt+Grt+Sil+Kfs	655		0.00		>641			676			672		

Total = 31 samples.

See text for discussion of mineral assemblages, uncertainties on distance, and petrological temperature estimates and uncertainties.

n: number of Raman spectra; R2: Raman R2 ratio; *T*(B02), *T*(A10r), *T*(A10c): RSCM temperatures from calibrations of Beyssac, Goffé, et al. (2002), Aoya et al. (2010) with A10r for regional and A10c for contact; *SD*: standard deviation; *SE*: standard error (*SE* is the *SD* divided by $\sqrt{N}$). See text for details.

Figure 10 of Pattison, Spear, BeBuhr, Cheney, and Guidotti (2002) shows that this reaction has a shallow negative slope in *P–T* space and is strongly dependent on bulk rock Mg/(Mg+Fe), most likely accounting for its progress in only some rocks.

4.2.3 | Pressure of contact metamorphism and isograd temperatures

Figure 3b shows a phase diagram calculated for the average Ballachulish carbonaceous argillite. The phase diagram differs from the Nelson phase diagram in Figure 3a because the Ballachulish bulk composition is more magnesian (Mg/(Mg+Fe) = 0.54 vs. 0.42), calcic (Ca/(Ca+Fe+Mg+Mn) = 0.12 vs. 0.01), and aluminous (A′= (Al-Na-2Ca-3K)/2 = 0.24 vs. 0.14) than the Nelson bulk composition. The isograd sequence in the aureole (cordierite; andalusite in some bulk compositions; K-feldspar; sillimanite) does not fit simply with the predicted phase equilibria in Figure 3b. For example, assuming an isobaric *P–T* path, passage through the MsAndBtCrd field in Figure 3b (corresponding to reaction B3) requires a higher pressure than is implied by the development of sillimanite upgrade of the development of andalusite+K-feldspar. Pattison et al. (2002) and Pattison and DeBuhr (2015) discussed difficulties in thermodynamically modelling reaction B3, which is sensitive to small changes in the mineral thermodynamic parameters. We, therefore, place greater emphasis on the development of andalusite+K-feldspar by reaction B2 than the sporadic development of Ms+And+Crd+Bt by reaction B3, and so favour a pressure of 3.0 kbar within a possible range of 2.7–3.3 kbar.

The temperature of the isograds in the Ballachulish aureole is based on the 3.0 kbar isobaric transect through the phase diagram in Figure 3b. The two reaction isograds that anchor the temperature profile in the Ballachulish aureole are similar to those in the Nelson aureole, namely the chlorite-out reaction (that at Ballachulish produces cordierite; reaction B1) and the muscovite-out reaction (that at Ballachulish produces andalusite+K-feldspar; reaction B2). For a pressure of contact metamorphism of 3 kbar, the temperature of reaction B1 is ~550°C. For a range of pressure of ±0.5 kbar, the temperature range varies by ±10°C. Incorporating some further uncertainty arising from uncertainty in the thermodynamic data, the preferred estimate for reaction B1 is 550 ± 20°C. For the muscovite-consuming reaction isograd (reaction B2), the estimated tempertature at 3.0 kbar is ~625°C. Over the pressure range of 2.5–3.5 kbar, the temperature range is 610–640°C (Figure 3b), which combined with some thermodynamic uncertainty results in an estimate of 625 ± 20°C for this reaction isograd. Despite using a different thermodynamic data set, the above estimates are the same as in Pattison (1989, 2006).

Temperatures of the highest grade rocks, between the K-feldspar-in isograd (reaction B2) and the igneous contact (Figure 2b), are constrained by the estimated contact temperature. The contact temperature in this part of the aureole is estimated to be ~700°C, based on the absence of high-grade mineral assemblages and absence of evidence for dehydration melting such as found elsewhere in the aureole, limiting temperatures to <750°C (Pattison, 1989). The greater degree of uncertainty on the contact temperature, compared to reaction isograds B1 and B2, yields an estimate of 700 ± 30°C.

The temperature estimates of reactions B1 and B2 are combined with the distance of the isograds from the contact (Figure 2b) to produce a temperature versus distance profile for Ballachulish in Figure 4b. Distances in Figure 4b and Table 3 are based on the grey section lines shown in Figure 2a,b. These were chosen to be perpendicular to the trace of the isograds and the intrusive contact, rather than at an oblique orientation as followed by the line of samples in Figure 2b, and thus more closely comparable to the thermal profiles in fig. 18.12 of Buntebarth (1991)

and fig. 11 of Pattison and Harte (1997). Samples were interpolated into the line of section in Figure 2a based on their position relative to the mapped isograds, yielding uncertainties of ±30 m. Numbered samples from Figure 2a, from well outside the aureole, have a larger uncertainty (±200 m). Similar to Nelson, temperature estimates of samples between, and outside, the two anchoring reaction isograds (filled circles in Figure 3b) are interpolated by eye, guided by the thermal profiles in Buntebarth (1991) and Pattison and Harte (1997), and thus are not independent estimates. The added temperature uncertainty arising from this interpolation method is thus estimated to be the same as described in Section 4.1.3 for Nelson (<±10°C between isograds, <±20°C outside the isograds). We note that the above estimates are not significantly compromised by possible variations in the shape or attitude of the intrusive contact as long as the mineral reactions (mapped isograds) record the variation in thermal conditions experienced by the rocks in the aureole.

4.2.4 | Temperature of host rocks outside the aureole

Temperature estimates for the regional rocks outside the aureole are based on the phase equilibria and geothermobarometry constraints described in Pattison (2013) and Pattison and Voll (1991) from rocks in the vicinity of the regional garnet isograd that lies a few kilometres northwest of the sample transect (Figure 2a). These cluster around 500°C at a pressure of 6–7 kbar. The gentle southeasterly increasing regional metamorphic gradient in the host rocks to the Ballachulish intrusion (Pattison, 2013) suggest that samples in the southeast of the area, upgrade of the garnet isograd, may have attained slightly higher temperatures than those in the northwest, downgrade of the garnet isograd. The preferred temperature estimate for the regional rocks is, therefore, 500 ± 20°C, shown as a band in Figure 4b.

This estimate assumes that there was no overstepping of the garnet-forming reaction due to kinetic impediments to garnet nucleation and growth. If overstepping was significant, the upper limit could be higher, although there is currently little consensus on the magnitude of overstepping of garnet formation, with estimates ranging from zero (George & Gaidies, 2017) to several tens of degrees (Kelly, Carlson, & Ketcham, 2013; Spear, Thomas, & Hallett, 2014). We favour the lower end of the range because of the absence of higher grade isograds within tens of kilometres of the area shown in Figure 2a (see also figs 1 and 2 of Pattison, 2013). A dashed line at 540°C has therefore been added to Figure 4b as an upper limit of the regional temperatures.

Two samples (92-4b and 92-65 in Figure 2 and Table 3) occur outside the cordierite-in isograd of the aureole (~550°C), but within ~500 m of it, and thus likely experienced contact metamorphic temperature that exceeded the regional temperature, but not enough to effect recrystallization. The estimated contact metamorphic temperature for the samples in Table 3 outside the cordierite isograd are based on the extrapolation of the thermal profile in Figure 4b.

5 | ABUNDANCE, MICROTEXTURES, AND RAMAN SPECTROSCOPY OF CM

5.1 | Abundance and microtextures of CM

Carbonaceous material is present in all lithologies examined from the two aureoles. Figure 5 depicts images of whole thin sections from different zones inside the aureoles, meaning upgrade of the garnet-in isograd at Nelson and upgrade of the cordierite-in isograd at Ballachulish, as well as rocks outside these isograds.

Whole-rock carbon contents from seven samples from the Nelson aureole in Figure 1b range from 0.04 to 1.22 wt %, corresponding to 0.05–1.5 vol.% graphite (appendix 1 of Pattison & Vogl, 2005). CM persists to the highest grades and shows no significant variation in abundance with grade, although rocks from the highest grade appear lighter coloured (Figure 5). In the Ballachulish aureole, Pattison (2006) examined optically 58 samples spanning the range of grade in the aureole. Thirteen were selected for whole-rock carbon analysis, of which five were chosen for carbon X-ray mapping in order to examine variations in the microscopic distribution and texture of CM (termed graphite in that study) with grade. The C content varies from 0.35 to 1.02 wt%, corresponding to 0.4–1.2 vol.% graphite. CM persists to the highest grades and shows no significant variation in abundance with grade, except for a possible decrease in the highest grade rocks (fig. 2 of Pattison, 2006), consistent with local "bleaching" of the rocks as noted at Nelson. Variable abundance of CM in rocks of the same grade was interpreted to reflect primary sedimentological heterogeneity. Thermodynamic calculations suggested that only 0.1–0.3 vol.% CM (graphitic carbon) was consumed during contact metamorphism (Pattison, 2006).

One of the main differences between the two settings is in the textures of the rocks outside the aureoles and in the most external part of the aureoles. At Nelson, the lowest grade rocks have a texture reminiscent of black shales observed in subgreenschist facies settings elsewhere. Conversely, in the case of Ballachulish, rocks from outside the aureole texturally look like schists with a clear foliation defined by chlorite and muscovite and CM.

Figure 6 presents representative photomicrographs illustrating microtextures of CM in the rocks outside the

TABLE 3 Summary of data for the Ballachulish aureole

Sample	Distance from contact (m) ±30 (Figure 2b) ±200 (Figure 2a)	Zone	Assemblage	*T* (°C) ± 20	R/C	*n*	R2 (avg)	*SD*	T_{B02} (°C)	*SD*	*SE*	T_{A10r} (°C)	*SD*	*SE*	T_{A10c} (°C)	*SD*	*SE*
		Regional samples															
92-63	2,800	I (Grt zone)	Ms+Chl	510	R	23	0.27	0.06	520	25	5	523	43	9	539	40	8
92-1A	2,500	I (Grt zone)	Ms+Chl	500	R	24	0.21	0.05	547	20	4	549	25	5	564	24	5
94-1/4	2,200	I (Bt zone)	Ms+Chl	490	R	21	0.23	0.03	539	14	3	538	17	4	554	16	4
92-65	1,600	I (Grt zone)	Ms+Chl	510/530	R/C	23	0.25	0.05	532	22	5	530	27	6	545	26	5
		Start of samples from transect															
92-4b	1,150	I	Ms+Chl	545	C	21	0.20	0.06	553	26	6	556	32	7	570	30	7
	1,100	***Cordierite+biotite-in isograd***		***550***													
92-4c	1,090	II	Ms+Chl+Crd+Bt	550	C	22	0.19	0.05	556	24	5	559	30	6	573	28	6
92-5	1,040	II	Ms+Chl+Crd+Bt	555	C	22	0.22	0.04	542	20	4	542	25	5	558	23	5
	1,000	Chlorite-out isograd		555													
92-8	920	III	Ms+Crd+Bt	560	C	26	0.22	0.06	542	28	5	542	34	7	557	32	6
92-9	850	III	Ms+Crd+Bt	565	C	23	0.21	0.05	547	24	5	549	29	6	564	28	6
92-10	720	III	Ms+Crd+Bt	575	C	25	0.20	0.07	550	30	6	552	38	8	567	35	7
92-12	650	III	Ms+Crd+Bt	580	C	19	0.20	0.06	554	26	6	557	32	7	572	31	7
94-4	550	III	Ms+Crd+Bt	585	C	21	0.21	0.05	549	22	5	551	28	6	566	26	6
92-13	550	III	Ms+Crd+Bt	585	C	23	0.21	0.05	549	22	5	551	28	6	566	26	5
94-5	500	III	Ms+Crd+Bt	590	C	24	0.19	0.05	556	20	4	559	25	5	574	24	5
	450	Andalusite-in isograd		595													
92-15	430	IV	Ms+Crd+Bt	595	C	12	0.21	0.06	547	26	7	548	32	9	563	30	9
93-15	430	IV	Ms+Crd+Bt	595	C	21	0.22	0.06	545	26	6	546	33	7	561	31	7
94-15	380	IV	Ms+Crd+And+Bt	600	C	29	0.24	0.04	536	19	4	535	23	4	550	22	4
94-7	330	IV	Ms+Crd+And+Bt	605	C	32	0.23	0.07	540	29	5	540	36	6	555	34	6
94-19	330	IV	Ms+Crd+And+Bt	605	C	27	0.22	0.06	542	27	5	543	33	6	558	31	6
92-16	300	IV	Ms+Crd+And+Bt	610	C	26	0.19	0.07	556	29	6	560	37	7	574	35	7
94-8	250	IV	Ms+Crd+And+Bt	620	C	27	0.19	0.06	555	25	5	558	32	6	573	30	6
94-9	240	IV	Ms+Crd+Bt	620	C	26	0.23	0.04	539	19	4	538	22	4	553	21	4
92-17	230	IV	Ms+Crd+And+Bt	625	C	34	0.21	0.06	547	27	5	548	33	6	563	32	5
	220	***K-feldspar-in isograd***		***625***													
94-10	210	V	Ms+Crd+And+Bt	625	C	34	0.21	0.06	549	25	4	550	31	5	565	30	5
94-11	190	V	Crd+And+Kfs+Ms+Bt	630	C	20	0.14	0.08	578	36	8	587	46	10	600	43	10
92-18	170	V	Crd+And+Kfs+Ms+Bt	640	C	35	0.21	0.06	549	28	5	551	35	6	566	33	6
92-19	130	V	Crd+And+Sil+Kfs+Ms	650	C	27	0.15	0.07	576	29	6	585	38	7	597	35	7
92-20	70	V	mig+Crd+Sil+And+Kfs	680	C		0.00		>641			676			672		
92-21	0	V	mig+Crd+Sil+And+Kfs	700	C		0.00		>641			676			672		

Total = 29 samples.

C = contact metamorphic. R = regional metamorphic. mig = rocks containing textures and structures suggestive of migmatisation by partial melting. Refer to Figure 2a,b for sample locations. See text for discussion of mineral assemblages, uncertainties on distance, and petrological temperature estimates and uncertainties. *n*: number of Raman spectra; R2: Raman R2 ratio; *T*(B02), *T*(A10r), *T*(A10c): RSCM temperatures from calibrations of Beyssac, Goffé, et al. (2002), Aoya et al. (2010) with A10r for regional and A10c for contact. *SD:* standard deviation; *SE*: standard error (*SE* is the *SD* divided by $\sqrt{N}$). See text for details.

aureoles, meaning downgrade of the first development of garnet and staurolite at Nelson and cordierite at Ballachulish. The Nelson rocks exhibit a very fine-grained mineralogy mostly composed of quartz and some phyllosilicates (muscovite, chlorite, and biotite). In these rocks, CM is either dispersed in the mineral matrix, or concentrated in diffuse planes within dark beds that may correspond to an original sedimentary structure. Regional rocks from outside

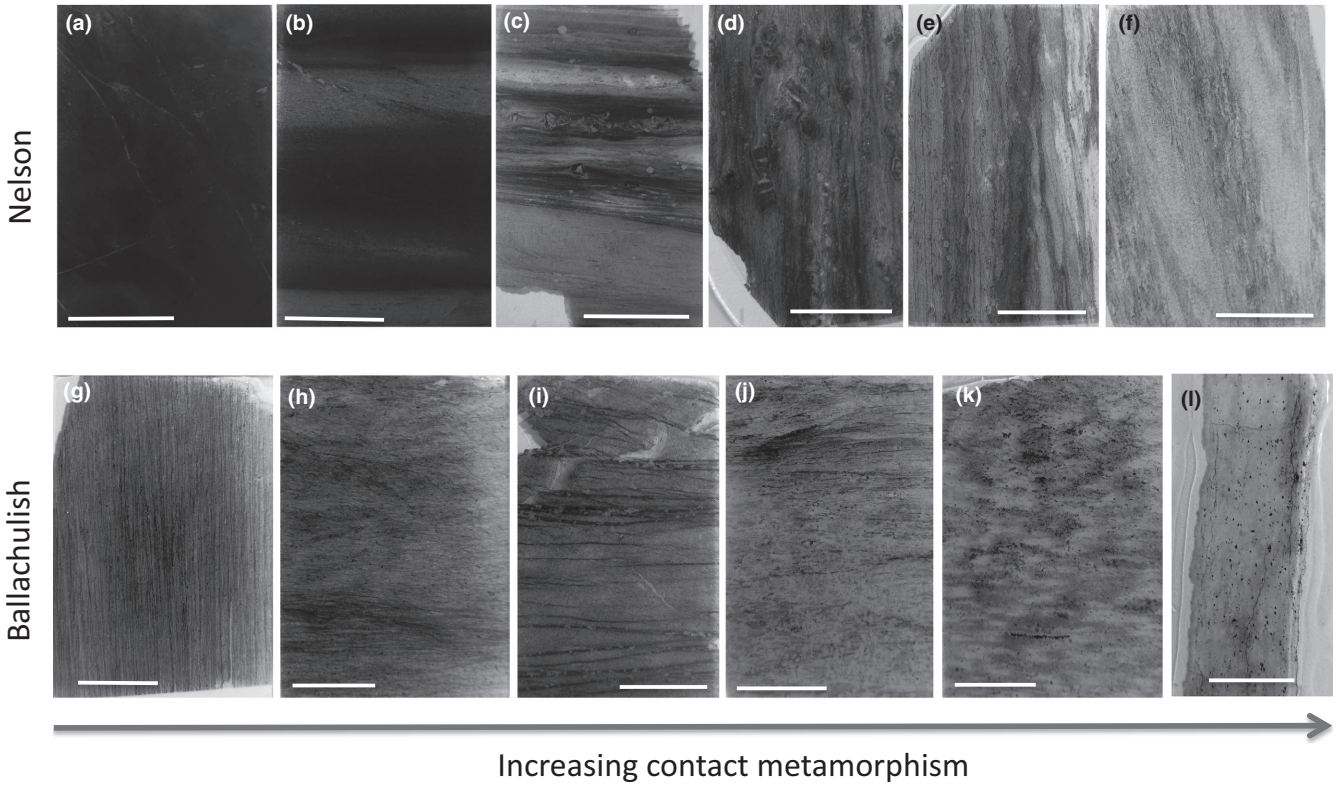

FIGURE 5 Scans of the rock thin sections for Nelson (top, a–f) and Ballachulish (bottom, g–l) in order of increasing metamorphic grade. Nelson a: 03-OC-9, b: 03-13, c: 93-5, d: 93-13, e: 93-16, f: 93-19a; Ballachulish g: 92-1A, h: 92-13, i: 94-19, j: 94-10, k: 92-19, l: 92-21. Sample locations for Nelson are shown in Figure 1b,c, and for Ballachulish in Figure 2a,b. Scale bar is 1 cm

the Ballachulish aureole are fine grained as well but systematically exhibit a marked foliation defined by aligned phyllosilicates (muscovite and chlorite) and CM.

Photomicrographs illustrating the microtexture of rocks within the Nelson aureole are provided in figs 5 and 6 of Pattison and Vogl (2005) and figs 2–10 of Pattison and Tinkham (2009). CM occurs finely dispersed in the matrix, as fine inclusions in garnet, staurolite, and andalusite porphyroblasts, the latter commonly chiastolitic, and in build-ups on the margins of andalusite porphyroblasts. Photomicrographs illustrating the microtexture of rocks within the Ballachulish aureole are provided in Pattison and Harte (1991) and in fig. 4 of Pattison (2006). Figure 5 of Pattison (2006) shows thin section carbon maps illustrating changes in the distribution and texture of CM going upgrade in the aureole. In regional rocks and in aureole rocks up to zone III (cordierite zone), CM is finely dispersed in the matrix of the rocks and in porphyroblasts of cordierite, where present. CM does not show any demonstrable contact metamorphic-associated textural modification until andalusite develops, where CM accumulates in build-ups on the margins of andalusite porphyroblasts. Overall, at Ballachulish, grains and aggregates of CM in the rock matrix become coarser grained and more widely separated as grade increases. These contact metamorphic-induced textural modifications of CM are superimposed on more pronounced mechanically induced features, such as segregations along cleavages and crenulations, that formed during regional deformation and garnet zone metamorphism prior to contact metamorphism. As discussed below, these pre-existing characteristics of the CM may have influenced the degree to which it equilibrated in the contact metamorphic event.

5.2 | Raman spectroscopy of CM in the Nelson and Ballachulish aureoles

Raman spectral analysis, including R2 ratio and RSCM temperature, together with the petrological temperature estimates, are presented in Tables 2 and 3, respectively, for the Nelson and Ballachulish aureoles. Figure 7 presents representative Raman spectra of CM obtained in the two aureoles. The Raman spectra of CM were collected from different textural settings in the rocks: diffuse CM in the mineral matrix, CM in the foliation planes, and CM inclusions in various porphyroblasts. No significant spectral differences among these populations were observed.

In both aureoles, CM outside the porphyroblast-in isograds exhibits a G band as well as the main defect bands D1 and D2, and the spectra are characteristic of disordered graphitic carbon. This graphitic carbon is relatively well ordered as indicated by the relatively low intensity of both D1 and

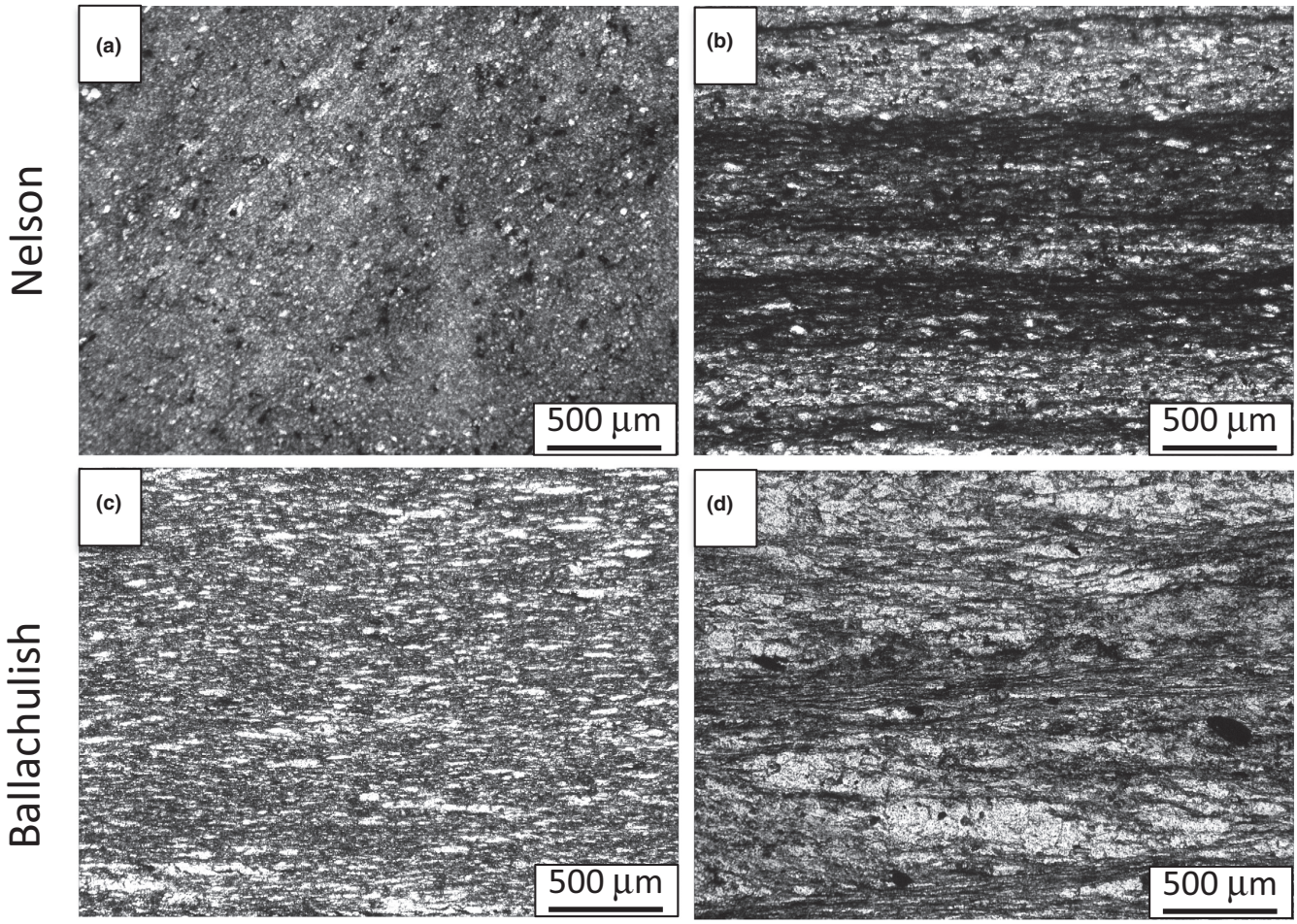

FIGURE 6 Photomicrographs of rocks from outside the garnet isograd of the Nelson aureole (a: 03-OC-9; b: 03-yc-06), and from outside the cordierite isograd of the Ballachulish aureole (c: 94-1/4; d: 92-1a)

D2 bands. However, inspection of the second-order region reveals an important difference between both settings. In the Nelson area, graphitic carbon did not reach the tridimensional structure of graphite, as the S1 band at ~2,700 cm^{-1} is still symmetric (top spectrum for Nelson in Figure 7). Conversely, all spectra retrieved from regional rocks outside the Ballachulish aureole exhibit an asymmetric S1 band, revealing that graphitic carbon has started to establish the tridimensional stacking (top spectrum for Ballachulish in Figure 7). Going upgrade in both aureoles, there is a decrease in both D1 and D2 bands up to complete disappearance in the highest grade zones close to the contact with the granitic intrusions (Figure 7). However, a conspicuous difference is that in the Nelson aureole the evolution of the Raman spectra is relatively smooth and progressive, whereas in the Ballachulish aureole the Raman spectra remain relatively constant up to the K-feldspar isograd, and then evolve rapidly to the spectra of perfect graphite. In both aureoles, a perfectly crystallized tridimensional graphite is observed in the highest grade samples at contact with plutonic rocks, as indicated by the absence of D1 and D2 defect bands in the spectra and confirmed by the systematic complete splitting in two bands of the main second-order band at ~2,700 cm^{-1} (indicative of ABAB tridimensional stacking).

A key observation is that the S1 band is symmetric at Nelson (one single band) and assymetric in Ballachulish (split in two bands) outside the contact aureoles. This means that CM is still turbostratic at Nelson (the graphitic planes are twisted and have not reached the ABAB tridimensionnal stacking of graphite), whereas it has started to reach the tridimensional structure of graphite in the case of Ballachulish. This splitting of the S1 band is a very sensitive marker for detecting tridimensionnal stacking in graphitic carbon (Lespade et al., 1984). It has been used and discussed for investigating the structure of graphitic carbons in metamorphic rocks (Beyssac, Rouzaud, Goffé, Brunet, & Chopin, 2002) and of synthetic graphitic carbons during pyrolysis (Bernard et al., 2010) in combination with TEM and/or X-ray or electron diffraction techniques. It has also been used to distinguish two kinds of graphitic carbons in the same high-*P* metasomatic rock: turbostratic graphitic carbon deriving from graphitization of organic matter

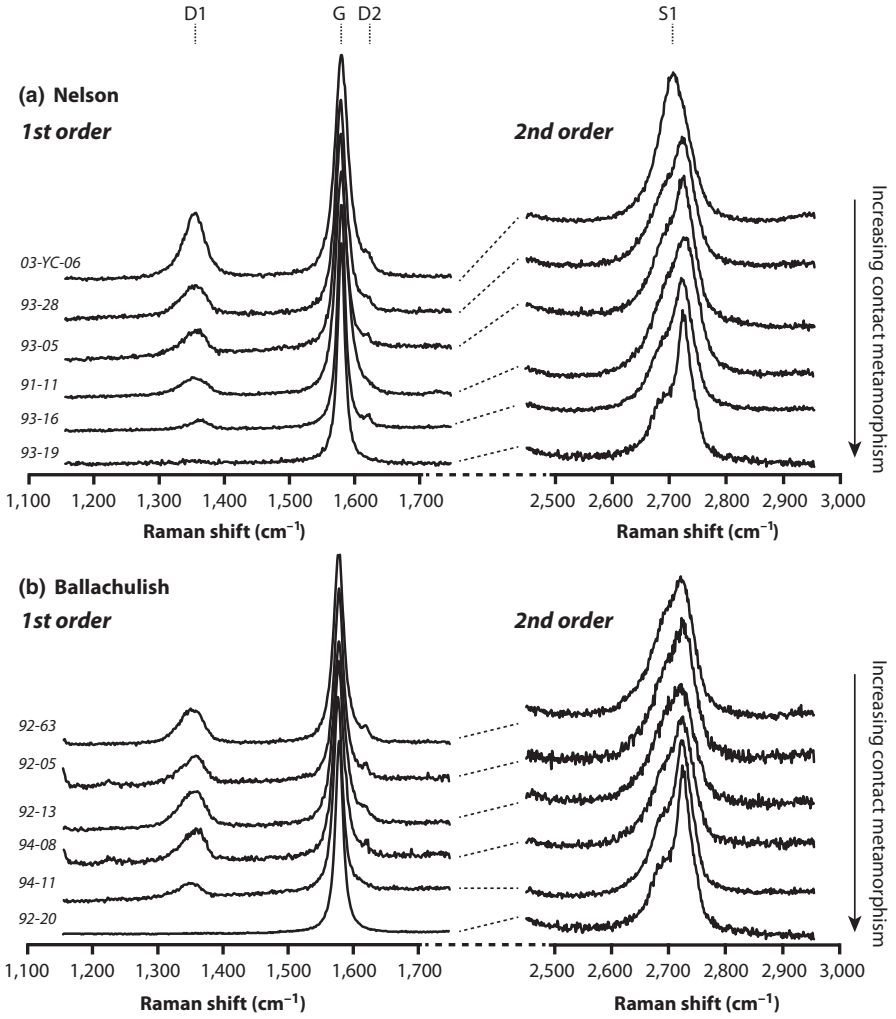

FIGURE 7 Representative Raman spectra for Nelson (a) and Ballachulish (b) with increasing contact metamorphism. For each spectrum, the first-order (1,100–1,700 cm^{-1}) and corresponding second-order regions (2,400–3,000 cm^{-1}) are presented. The first-order region gives an insight on the degree of graphitization and the second-order region on the 3D stacking of graphitic CM

in the host unmetasomatised rock versus hydrothermal graphitic carbon formed by infiltration-driven reduction of carbonates during subduction (Galvez et al., 2013). In CM from metamorphic settings, this splitting of the S1 band is typically observed for a R2 ratio of ~0.3 (Beyssac, Goffé, et al., 2002) corresponding to temperatures in the range 500–550°C (Beyssac, Goffé, et al., 2002; Wopenka & Pasteris, 1993). This corresponds to the range of R2 ratio observed in the rocks outside the Nelson and Ballachulish aureoles. In addition, this suggests that at Nelson the contact metamorphic overprint outside the aureole did not trigger the local tridimensional ordering of CM although it was likely not far to do so as this splitting of S1 rapidly appears within the contact aureole (i.e., above the Grt-in isograd).

Evolution of the R2 ratio in the two aureoles is illustrated in Figure 8 and confirms the qualitative evolution of graphitization described above from the visual inspection of Raman spectra. At Nelson (Figure 8a), R2 is relatively constant outside the porphyroblast-in isograd at a value ~0.25. Going upgrade in the aureole, R2 decreases progressively from ~0.25 to 0.0, the value of perfect graphite, with no abrupt changes including at the main mineral isograds. Locally some outliers exhibiting higher or lower R2 values are observed, showing that graphitization proceeds with some heterogeneity within the aureole. The standard deviation for the average R2 value in each sample, in the range 0.04–0.07, shows no systematic pattern with distance to the pluton, showing that the within-sample structural heterogeneity of CM is relatively uniform in all these rocks along the transect. At Ballachulish (Figure 8b), the range in R2 for the regional rocks outside the cordierite-in isograd is similar to that for the lowest grade rocks at Nelson, but slightly more heterogeneous towards lower values (Figure 8; Tables 2 and 3). R2 remains relatively unchanged and constant through the aureole until approximately the K-feldspar isograd, within 200 m of the igneous contact, where it decreases abruptly to the null value of graphite. As at Nelson, the standard deviation for R2 values of individual samples is more or less constant as a function of distance to the pluton, in the range 0.04–0.07, showing that the structural heterogeneity of CM is relatively uniform in all these rocks.

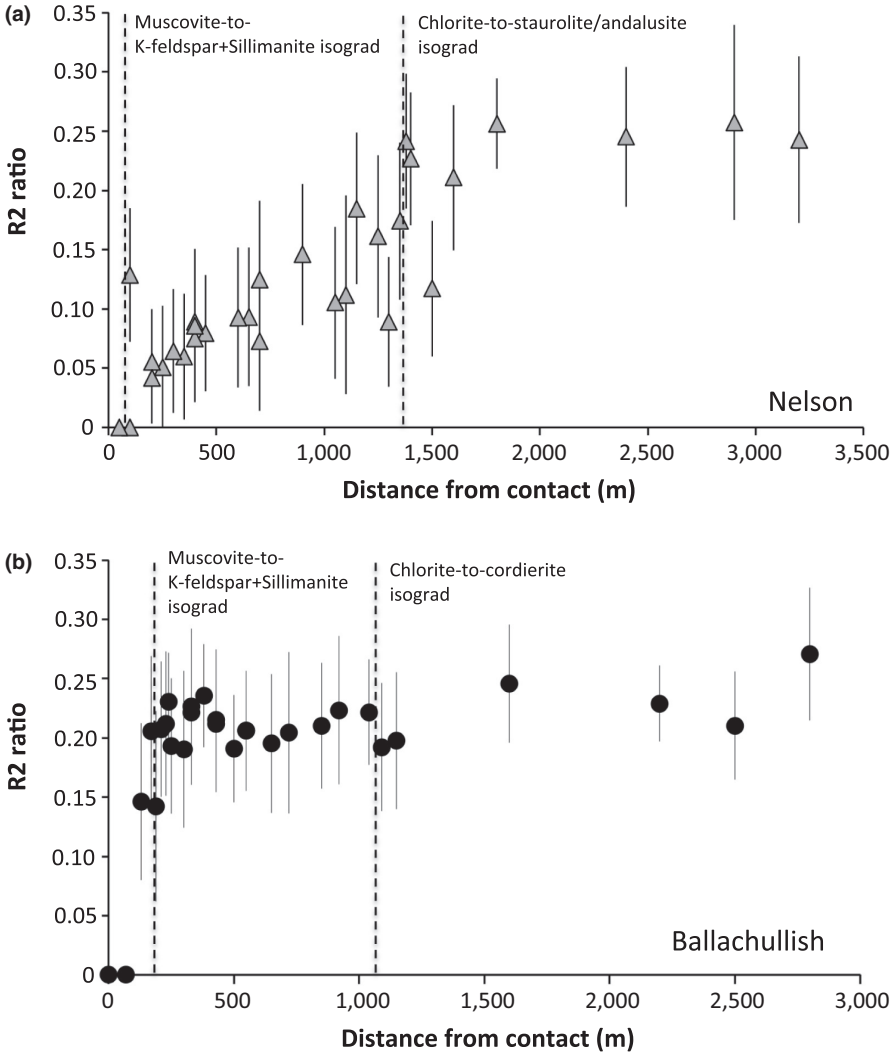

FIGURE 8 (a) Evolution of the R2 ratio with distance to the intrusion for the Nelson aureole. Note the progressive and continuous decrease in R2 towards the intrusion (error bar is *SD* for n spectra, see text and Table 2). (b) Evolution of the R2 ratio with distance to the intrusion for the Ballachulish aureole (error bar is *SD* for n spectra, see text and Table 3). In (a) and (b), R2 value of 0 indicates presence of pristine graphite (see text)

6 | DELAYED RECRYSTALLIZATION OF PREVIOUSLY METAMORPHOSED CM AT BALLACHULISH

Several studies have compared graphitization patterns between contact and regional metamorphism. Earlier studies used X-ray diffraction to investigate the structure of CM extracted from rocks and concluded that there might be a slight delay of graphitization in contact aureoles when compared to rocks of equivalent grade in a regional metamorphic gradient (Grew, 1974; Okuyama-Kusunose & Itaya, 1987), or no real difference except in the outer low-grade parts of contact aureoles (Wada et al., 1994). Alternatively, more recent studies used Raman microspectroscopy to quantify in situ the CM degree of graphitization and were focused on calculating RSCM temperatures (Aoya et al., 2010; Delchini, Lahfid, Plunder, & Michard, 2016; Hilchie & Jamieson, 2014). Based on RSCM temperatures, they all concluded that graphitization proceeds to the same degree for a given metamorphic grade in both contact and regional metamorphic settings. In the studies by Aoya et al. (2010), Hilchie and Jamieson (2014), and Delchini et al. (2016), contact metamorphism was superposed on rocks that had already experienced greenschist facies regional metamorphism with temperature estimated in the range 300–400°C. Reasons for different conclusions among the early X-ray diffraction-based studies and later studies based on Raman microspectroscopy are unclear and it might be a consequence of an analytical discrepancy as X-ray diffraction is a bulk technique, whereas Raman microspectroscopy only probes a few μm^3. It can be a consequence of sample preparation as well as X-ray diffraction requires mechanical and chemical extraction of CM from the rocks which may alter the fragile structure of highly ordered graphitic carbon like those typically observed in contact aureoles. Regardless of the characterization technique, the graphitization pattern in the aureoles is systematically progressive and continuous with increasing grade. This situation corresponds to the pattern of

graphitization observed in the Nelson aureole, where the intrusion was emplaced in regional rocks that were essentially unmetamorphosed (subgreenschist facies; see Section 4.1).

Two contrasted patterns are observed for the progress of graphitization with increasing contact metamorphism in the Nelson and Ballachulisch aureoles. Nelson aureole exhibits a progressive and continuous steady crystallization of CM following the progressive temperature increase towards the granitic intrusion with no noticeable break at the main mineral isograds. Some local heterogenity is observed, the causes of which are unknown. Conversely, the pattern of graphitization at Ballachulish is different. Based on Raman spectroscopy proxies (R2 ratio, shape of the S1 band), CM structure seems to remain relatively uniform throughout the transect up to ~200 m from the contact with the intrusion, at approximately the K-feldspar isograd; at that point, there is an abrupt increase in graphitization. In both settings, perfect graphite with tridimensionnal stacking is observed in the highest grade rocks close to the contact with the intrusion.

Inspection of the rock textures (Figure 5) and microtextures (Figure 6) reveals a marked difference for the rocks outside the aureole although the R2 ratio for CM is nearly the same in both settings: the Nelson rocks have a textural habit similar to low-grade metamorphic rocks, whereas the Ballachulish rock has the habit of a micashist with a well-marked foliation. Nonetheless, rocks sampled downgrade of the porphyroblast-in isograd at Nelson were also submitted to the thermal effects of contact metamorphism as recorded by RSCM thermometry. This result is consistent with the regional isograd pattern and with the random texture of biotite in the low-grade rocks which is suggestive of relatively static contact metamorphism (see discussion in Section 4.1.4).

At Ballachulish, CM had already reached locally the tridimensional ordering of graphite before the intrusion and formation of the contact aureole. This pretransformation of CM is likely responsible for the sluggish recrystallization and delayed graphitization observed in this aureole. Tridimensional ordering of graphitic carbon means that the graphitic planes are wide enough to develop strong long range Van Der Waals interactions over large areas among them to get closer and have a d_{002} spacing tending towards 3.35 angstroms as detected by X-ray diffraction in perfect graphite. However, this "CM starting material" was still partially disordered as attested by the presence of D1 and D2 bands in the first-order region as well as by the incomplete splitting of the S1 band in the second-order region. In reality, at the nanoscale, such CM was likely microtexturally and structurally heterogeneous, containing some nucleation zones for the development and propagation of tridimensional ordering as observed in other metamorphic settings by high-resolution TEM (Beyssac, Rouzaud, et al., 2002; Buseck & Huang, 1985). Such heterogeneous nucleation and propagation of graphitization at the nanoscale has been reproduced and observed in synthetic CM retrieved from high-*P* and high-*T* experiments (Beyssac, Brunet, et al., 2003).

It appears that further graphitization of such pretextured CM required a significant temperature overstepping compared to other settings where "CM starting material" was still turbostratic (Nelson, this study; Aoya et al., 2010; Delchini et al., 2016; Hilchie & Jamieson, 2014). The final stage of graphitization mostly consists of polymerization (extending the graphitic planes) and tridimensional ordering of the graphitic planes. At Ballachulish, this final graphitization stage may have required additional energy to reorganize the pre-existing strong, but imperfect, structure compared to the steady graphitization observed at Nelson and other aureoles. Interestingly, graphitization of this CM at Ballachulish starts at the K-feldspar isograd which corresponds to the breakdown of muscovite and to a major fluid release which may have had a role in triggering graphitization at Ballachulish by possibly lowering some of the kinetic barriers. However, no significant break in graphitization is observed at the chlorite-out isograd which corresponds to the biggest fluid release (56% of water released vs. 20% at Ms-out; see fig. 8 of Pattison, 2006). We do not have a clear mechanism at this stage to explain this delayed graphitization which could alternatively be the consequence of an Arrhenius thermal threshold; further work including investigations in other natural settings or experimental work is needed to pursue these ideas.

7 | IMPLICATIONS FOR RSCM THERMOMETRY

7.1 | RSCM temperatures in the Ballachulish and Nelson aureoles

The R2 values can be used to calculate peak metamorphic temperature with equations calibrated using samples affected by regional metamorphism (Aoya et al., 2010 their "regional" calibration; Beyssac, Goffé, et al., 2002) or contact metamorphism (Aoya et al., 2010—their "contact" calibration). The temperature results for Nelson and Ballachulish, in combination with temperature estimates retrieved from petrology (see above), are given in Tables 2 and 3, and shown in Figure 4a,b respectively.

For initial analysis, we discuss temperature calculated with the calibration by Beyssac, Goffé, et al. (2002); comparison with the calibrations by Aoya et al. (2010) follows. In both aureoles, RSCM temperature for the remote samples collected far from the intrusions are quite

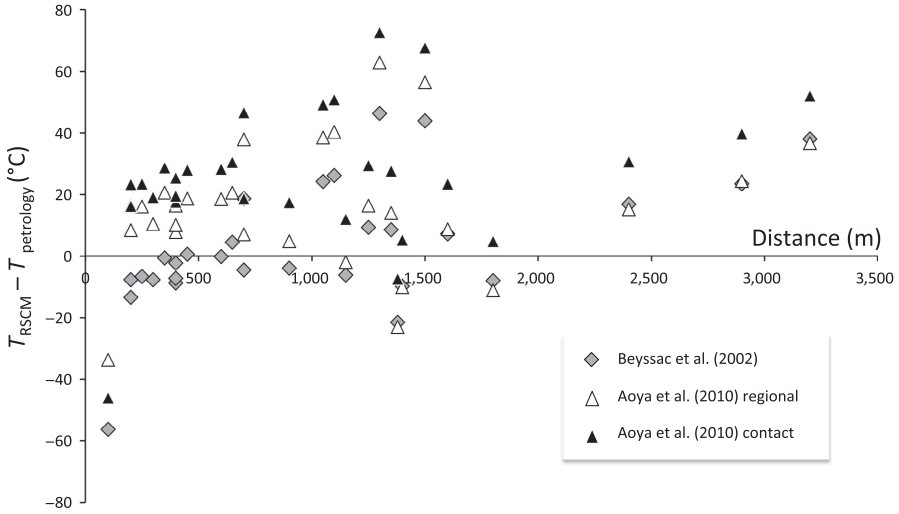

FIGURE 9 Comparison of temperatures between the various RSCM calibrations and petrology by calculating the difference between RSCM temperature and petrology temperature for each sample versus the distance to the intrusion for the Nelson aureole. Uncertainty for RSCM thermometry is ±50°C (see text)

similar at ~525–535°C for Nelson and are slightly higher but more dispersed for Ballachulish in the range 520–550°C. As discussed above, these temperatures likely reflect contact metamorphism associated with the Nelson intrusion while they represent preintrusion regional metamorphism at Ballachulish. At the other extreme, perfect graphite is observed (no D1 defect band, R2 = 0.0, splitting of the S1 band) indicating temperature higher than 640°C. Due to the linear character of the relationship between the R2 parameter and temperature, the evolution of temperature in between these end-members follows the same pattern described above for the evolution of R2 in both aureoles: progressive within the transect for Nelson, and no change until an abrupt increase in the innermost zones at Ballachulish. This situation contrasts with the petrological constraints that show a progressive increase in temperature as the contact is approached in both aureoles.

7.2 | Comparison with other areas and RSCM thermometry in contact aureoles: testing calibrations

The RSCM thermometry was initially calibrated by using petrological data from samples affected by a single regional metamorphic event (Beyssac, Goffé, et al., 2002; here B02) with an estimated uncertainty of ±50°C. This initial calibration was a linear fit between the R2 ratio and petrological temperature and likely slightly underestimated temperature at values higher than 600–620°C (Negro, Beyssac, Goffé, Saddiqi, & Bouybaouene, 2006); a quadratic equation was not chosen by Beyssac, Goffé, et al. (2002) because of a lack of data at such high temperatures. Aoya et al. (2010) modified this initial calibration for regional metamorphism (referred to here as A10r) by using a quadratic equation to fit the data set from Beyssac, Goffé, et al. (2002), but added no new data. For contact metamorphism, Aoya et al. (2010) developed a calibration based on the study of contact aureoles in Japan for which temperature is estimated from the combination of various thermometers for anchor points and interpolation for samples in-between based on thermal modelling (referred to here as A10c); an approach similar in principle to ours for Ballachulish and Nelson. Figure 4a,b shows that the RSCM temperatures retrieved by the two calibrations, A10r and A10c, are only slightly different than those obtained with the B02, with systematically greater difference between B02/A10r versus A10c. In Figure 9, the results of the three calibrations are compared with temperatures from petrology for the Nelson aureole. We note that (a) the B02 calibration is relatively close to the A10r calibration for the samples outside the contact aureole and that the A10c calibration is higher, (b) the A10r temperatures generally fall in the middle range of B02 and A10c within the contact aureole, and (c) there is a generally better agreement of the B02 calibration with the petrological constraints except for the highest temperature points. At Ballachulish, the B02 calibration is very close to the A10r calibration for the samples outside the contact aureole while the A10c is then higher by ~20°C, but we do not make a comparison within the aureole as RSCM thermometry does not appear to be applicable there as discussed above.

The A10r calibration generally yields higher temperature estimates above 600°C due to its quadratic nature, but the constraints in this temperature range in the B02 data set used by A10r are limited. The differences between B02 and A10c likely come from the temperature estimates by petrology used as reference for the calibration (all petrological estimates for B02 and a combination of petrological estimates and thermal modelling for A10c).

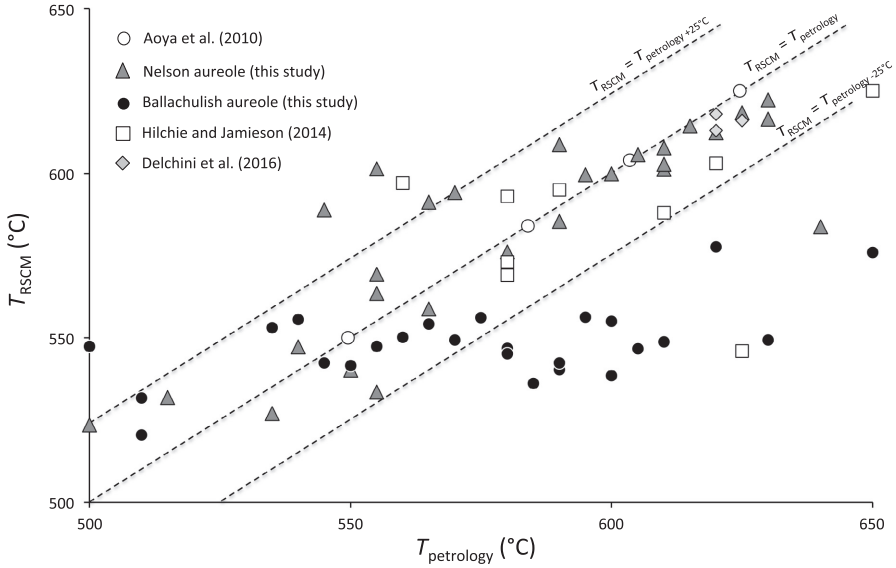

FIGURE 10 Comparison of RSCM temperatures versus reference temperatures standing for temperatures quantified by conventional petrology and thermal modelling (Nelson and Ballachulish, this study), mineral assemblage and pseudosections (aureole in Morocco by Delchini et al., 2016), mineral assemblage and conventional geothermobarometry (aureoles in Japan by Aoya et al., 2010), thermal modelling with input from conventional petrology, and RSCM thermometry (aureole in Canada by Hilchie & Jamieson, 2014). The 1:1 line is depicted as well as lines representing 1:1 ± 25°C. Uncertainty for RSCM thermometry is ±50°C (see text)

One may ask the reason for using different calibrations between contact and regional metamorphism as all recent studies showed no kinetic effect on graphitization on such time-scales. There is actually an excellent agreement between RSCM estimates whatever the calibration (B02, A10r, or A10c) and petrological data and/or temperature retrieved from thermal modelling (Aoya et al., 2010; Delchini et al., 2016; Hilchie & Jamieson, 2014). This is in agreement with a recent kinetic modelling of graphitization which shows that this transformation proceeds rapidly in most metamorphic settings (Nakamura et al., 2017). In very short time-scale heating events (100–500 years), such as heating induced by a sill intrusion, graphitization may be limited by the duration of the thermal event (Mori, Mori, Wallis, Westaway, & Annen, 2016) but this is different from the time-scale for contact metamorphism developed in contact aureoles due to the emplacement of igneous intrusions on the km scale, which is typically hundreds of thousands of years for rocks raised to >500°C, such as Nelson and Ballachulish (see references above). This point is further supported by a plot of RSCM temperature data in contact aureole versus reference temperature estimates from the same source paper (this study; Aoya et al., 2010; Delchini et al., 2016; Hilchie & Jamieson, 2014) presented in Figure 10. Reference temperature is an independent petrological estimate of temperature, except for the Halifax aureole in Nova Scotia, where it is quantified from thermal modelling with input from conventional petrology and RSCM thermometry (Hilchie & Jamieson, 2014). Apart from Ballachulish, the data mainly fall around the 1:1 line within an envelope of ±25°C except for a few outliers. The case of Ballachulish is different and likely due to the complex polymetamorphic history of these rocks as discussed above.

8 | CONCLUSIONS: SOME IMPLICATIONS FOR RSCM THERMOMETRY

The graphitization pattern and calculated RSCM temperatures were examined in two well-characterized contact aureoles with contrasting metamorphic histories. In the case of Nelson where contact metamorphism overprints essentially unmetamorphosed rocks, the graphitization pattern is controlled by the temperature increase in the contact aureole. The RSCM thermometry nicely records the thermal signature of the contact metamorphism and is in good agreement with petrological data. Interestingly, RSCM thermometry showed that rocks outside the contact aureole, as defined by the porphyroblast-in isograd, were likely affected by the same contact metamorphic imprint even though there is little mineralogical evidence. A similar observation was made by Hilchie and Jamieson (2014) which opens new avenues for tracking the thermal overprint of intrusions with RSCM thermometry in rocks outside the porphyroblast-bearing zones where mineralogical changes are more subtle and harder to quantify petrologically.

The case of Ballachulish is different as the intrusion was emplaced into rocks that had already been affected by high-grade garnet zone (lower amphibolite facies) metamorphism at >500°C. We have shown that this regional metamorphism transformed the CM into a highly ordered material at the threshold of tridimensional ordering of graphite prior to contact metamorphism. Recrystallization of CM and graphitization in the Ballachulish aureole was delayed likely due to the pretexturation of CM during regional metamorphism with the result that the RSCM thermometry underestimates peak temperature in the aureole. Such a delay in graphitization has not been observed elsewhere in the case of two successive regional metamorphic events even if the first one reached high-grade conditions: this was shown in the central part of the southern Alps of New Zealand (Beyssac, Cox, Vry, & Herman, 2016) or in some parts of the European Alps (Wiederkehr, Bousquet, Ziemann, Berger, & Schmid, 2011). Note that in these settings, the successive regional metamorphisms are mostly due to burial related to subduction and/or collision. This makes the situation different from Ballachulish where a thermal perturbation due to a hot intrusion locally overprints a pre-existing regional metamorphism. In any case, the Ballachulish case study shows that RSCM thermometry needs to be applied with caution in polymetamorphic settings involving an early event that exceeded ~500°C.

ACKNOWLEDGEMENTS

O.B. acknowledges funding from Sorbonne Université (PERSU program) and the City of Paris (Emergence Program). D.P. acknowledges NSERC Discovery Grant 037233. We thank L.J. Hilchie and an anonymous reviewer for thorough and constructive reviews and D. Robinson for editorial handling.

ORCID

Oliver Beyssac http://orcid.org/0000-0001-8879-4762
David R. M. Pattison http://orcid.org/0000-0001-5817-6373
Franck Bourdelle http://orcid.org/0000-0002-7136-8692

REFERENCES

Aoya, M., Kouketsu, Y., Endo, S., Shimizu, H., Mizukami, T., Nakamura, D., & Wallis, S. (2010). Extending the applicability of the Raman carbonaceous-material geothermometer using data from contact metamorphic rocks. *Journal of Metamorphic Geology*, *28*, 895–914. https://doi.org/10.1111/j.1525-1314.2010.00896.x

Archibald, D. A., Glover, J. K., Price, R. A., Carmichael, D. M., & Farrar, E. (1983). Geochronology and tectonic implications of magmatism and metamorphism, Southern Kootenay Arc and neighbouring regions, southeastern British Columbia, Part I: Jurassic to Mid-Cretaceous. *Canadian Journal of Earth Sciences*, *20*, 1891–1913. https://doi.org/10.1139/e83-178

Bernard, S., Beyssac, O., Benzerara, K., Findling, N., Tzvetkov, G., & Brown, G. E. Jr. (2010). XANES, Raman and XRD signatures of anthracene-based cokes and saccharose-based chars submitted to high temperature pyrolysis. *Carbon*, *48*, 2506–2516. https://doi.org/10.1016/j.carbon.2010.03.024

Beyssac, O., Bollinger, L., Avouac, J. P., & Goffé, B. (2004). Thermal metamorphism in the lesser Himalaya of Nepal determined from Raman spectroscopy of carbonaceous material. *Earth and Planetary Science Letters*, *225*, 233–241. https://doi.org/10.1016/j.epsl.2004.05.023

Beyssac, O., Brunet, F., Petitet, J. P., Goffé, B., & Rouzaud, J. N. (2003). Experimental study of the microtextural and structural transformations of carbonaceous materials under pressure and temperature. *European Journal of Mineralogy*, *15*, 937–951. https://doi.org/10.1127/0935-1221/2003/0015-0937

Beyssac, O., Cox, S. C., Vry, J. K., & Herman, F. (2016). Peak metamorphic temperature and thermal history of the Southern Alps (New Zealand). *Tectonophysics*, *676*, 229–249. https://doi.org/10.1016/j.tecto.2015.12.024

Beyssac, O., Goffé, B., Chopin, C., & Rouzaud, J. N. (2002). Raman spectra of carbonaceous material in metasediments: A new geothermometer. *Journal of Metamorphic Geology*, *20*, 859–871. https://doi.org/10.1046/j.1525-1314.2002.00408.x

Beyssac, O., Goffé, B., Petitet, J. P., Froigneux, E., Moreau, M., & Rouzaud, J. N. (2003). On the characterization of disordered and heterogeneous carbonaceous materials by Raman spectroscopy. *Spectrochimica Acta Part A*, *59*, 2267–2276. https://doi.org/10.1016/S1386-1425(03)00070-2

Beyssac, O., & Lazzeri, M. (2012). Application of Raman spectroscopy to the study of graphitic carbons in the Earth Sciences. In J. Dubessy, M.-C. Caumon & F. Rull (Eds.), *Applications of Raman spectroscopy to earth sciences and cultural heritage*. *EMU Notes in Mineralogy*, *12*, 415–454.

Beyssac, O., Rouzaud, J. N., Goffé, B., Brunet, F., & Chopin, C. (2002). Graphitization in a high-pressure, low-temperature metamorphic gradient: A Raman microspectroscopy and HRTEM study. *Contributions to Mineral Petrology*, *143*, 19–31. https://doi.org/10.1007/s00410-001-0324-7

Buntebarth, G. (1991). Thermal models of cooling. In G. Voll, J. Töpel, D. R. M. Pattison & F. Seifert (Eds.), *Equilibrium and kinetics in contact metamorphism: The Ballachulish igneous complex and its thermal aureole* (pp. 379–404). Heidelberg, Germany: Springer Verlag. https://doi.org/10.1007/978-3-642-76145-4

Buseck, P. R., & Beyssac, O. (2014). From organic matter to graphite: Graphitization. *Elements*, *10*(6), 421–426. https://doi.org/10.2113/gselements.10.6.421

Buseck, P. R., & Huang, B.-J. (1985). Conversion of carbonaceous material to graphite during metamorphism. *Geochimica et Cosmochimica Acta*, *49*, 2003–2016. https://doi.org/10.1016/0016-7037(85)90059-6

Busemann, H., Alexander, M. O'D., & Nittler, L. R. (2007). Characterization of insoluble organic matter in primitive meteorites by microRaman spectroscopy. *Meteoritics & Planetary Science*, *42*, 1387–1416. https://doi.org/10.1111/j.1945-5100.2007.tb00581.x

Coggon, R., & Holland, T. J. B. (2002). Mixing properties of phengitic micas and revised garnet-phengite thermobarometers. *Journal*

of Metamorphic Geology, *20*, 683–696. https://doi.org/10.1046/j.1525-1314.2002.00395.x

Connolly, J. A. D., & Cesare, B. (1993). C-O-H-S fluid compositions and oxygen fugacity in graphitic metapelites. *Journal of Metamorphic Geology*, *11*, 379–388. https://doi.org/10.1111/j.1525-1314.1993.tb00155.x

Cook, F. A., Green, A. G., Simony, P. S., Price, R. A., Parrish, R. R., Milkereit, B., … Patenaude, C. (1988). Lithoprobe seismic reflection structure of the southeastern Canadian Cordillera: Initial results. *Tectonics*, *7*, 157–180. https://doi.org/10.1029/TC007i002p00157

De Capitani, C., & Brown, T. H. (1987). The computation of chemical equilibria in complex systems containing non-ideal solutions. *Geochimica et Cosmochimica Acta*, *51*, 2639–2652. https://doi.org/10.1016/0016-7037(87)90145-1

De Capitani, C., & Petrakakis, K. (2010). The computation of equilibrium assemblage diagrams with Theriak/Domino software. *American Mineralogist*, *95*, 1006–1016. https://doi.org/10.2138/am.2010.3354

Delchini, S., Lahfid, A., Plunder, A., & Michard, A. (2016). Applicability of the RSCM geothermometry approach in a complex tecto-metamorphic context (Variscan orogen, Morocco). *Lithos*, *256–257*, 1–12. https://doi.org/10.1016/j.lithos.2016.04.007

Ferry, J. M. (1996). Prograde and retrograde fluid flow during contact metamorphism of siliceous carbonate rocks from the Ballachulish aureole, Scotland. *Contributions to Mineralogy and Petrology*, *124*, 235–254. https://doi.org/10.1007/s004100050189

Fraser, G. L., Pattison, D. R. M., & Heaman, L. M. (2004). Age of the Ballachulish and Glencoe Igneous Complexes (Scottish Highlands), and paragenesis of zircon, monazite and baddeleyite in the Ballachulish Aureole. *Journal of the Geological Society of London*, *161*, 447–462. https://doi.org/10.1144/0016-764903-018

Galvez, M. E., Beyssac, O., Martinez, I., Benzerara, K., Chaduteau, C., Malvoisin, B., & Malavieille, J. (2013). Graphite formation by carbonate reduction during subduction. *Nature Geoscience*, *6*(6), 473–477. https://doi.org/10.1038/ngeo1827

Galy, V., Beyssac, O., France-Lanord, C., & Eglinton, T. (2008). Selective recycling of graphite during Himalayan erosion: A geological stabilisation of C in the crust. *Science*, *322*, 943–945. https://doi.org/10.1126/science.1161408

George, F. R., & Gaidies, F. (2017). Characterisation of a garnet population from the Sikkim Himalaya: Insights into the rates and mechanisms of porphyroblast crystallization. *Contributions to Mineralogy and Petrology*, *172*, 57. https://doi.org/10.1007/s00410-017-1372-y

Ghosh, D. K. (1995). U-Pb geochronology of Jurassic to early Tertiary granitic intrusives from the Nelson-Castlegar area, southeastern British Columbia, Canada. *Canadian Journal of Earth Sciences*, *32*, 1668–1680. https://doi.org/10.1139/e95-132

Grew, E. S. (1974). Carbonaceous material in some metamorphic rocks of New England and other areas. *The Journal of Geology*, *82*, 50–73. https://doi.org/10.1086/627936

Harte, B., Pattison, D. R. M., Heuss-Assbichler, S., Hoernes, S., Masch, L., & Strong, D. F. (1991). Evidence of fluid phase behaviour and controls in the intrusive complex and its aureole. In G. Voll, J. Töpel, D. R. M. Pattison & F. Seifert (Eds.), *Equilibrium and kinetics in contact metamorphism: The Ballachulish igneous complex and its thermal aureole* (pp. 405–422). Heidelberg, Germany: Springer Verlag. https://doi.org/10.1007/978-3-642-76145-4

Hilchie, L. J., & Jamieson, R. A. (2014). Graphite thermometry in a low-pressure contact aureole, Halifax, Nova Scotia. *Lithos*, *208–209*, 21–33. https://doi.org/10.1016/j.lithos.2014.08.015

Holland, T. J. B., & Powell, R. (1998). An internally consistent thermodynamic data set for phases of petrological interest. *Journal of Metamorphic Geology*, *16*, 309–344.

Holland, T. J. B., & Powell, R. (2003). Activity-composition relations for phases in petrological calculations: An asymmetric multicomponent formulation. *Contributions to Mineralogy and Petrology*, *145*, 492–501. https://doi.org/10.1007/s00410-003-0464-z

Holland, T. J. B., & Powell, R. (2011). An improved and extended internally consistent thermodynamic dataset for phases of petrological interest, involving a new equation of state for solids. *Journal of Metamorphic Geology*, *29*, 333–383.

Kelly, E. D., Carlson, W. D., & Ketcham, R. A. (2013). Magnitudes of departure from equilibrium during regional metamorphism of porphyroblastic rocks. *Journal of Metamorphic Geology*, *31*, 981–1002. https://doi.org/10.1111/jmg.12053

Kretz, R. (1983). Symbols for rock-forming minerals. *American Mineralogist*, *68*, 277–279.

Lespade, P., Marchand, A., Couzi, M., & Cruege, F. (1984). Characterization of carbon materials with Raman microspectrometry. *Carbon*, *22*, 375–385. https://doi.org/10.1016/0008-6223(84)90009-5

Little, H. W. (1960). Nelson Map-area, West-half, British Columbia. *Geological Survey of Canada, Memoir*, *308*, 205.

Morgan, A. L. (2016). *Metamorphism of the Rossland Group metabasalts and metapelites, southeastern British Columbia*. Unpublished BSc thesis, University of Calgary, 131 pp.

Mori, H., Mori, N., Wallis, S., Westaway, R., & Annen, C. (2016). The importance of heating duration for Raman CM thermometry: Evidence from contact metamorphism around the Great Whin Sill intrusion, UK. *Journal of Metamorphic Geology*, *35*, 165–180.

Nakamura, Y., Yoshino, T., & Satish-Kumar, M. (2017). An experimental kinetic study on the structural evolution of natural carbonaceous material to graphite. *American Mineralogist*, *102*, 135–148. https://doi.org/10.2138/am-2017-5733

Negro, F., Beyssac, O., Goffé, B., Saddiqi, O., & Bouybaouene, M. (2006). Thermal structure of the Alboran Domain in the Rif (northern Morocco) and the Western Betics (southern Spain). Constraints from Raman Spectroscopy of Carbonaceous Material. *Journal of Metamorphic Geology*, *24*, 309–327. https://doi.org/10.1111/j.1525-1314.2006.00639.x

Okuyama-Kusunose, Y., & Itaya, T. (1987). Metamorphism of carbonaceous material in the Tono contact aureole, Kitakami Mountains, Japan. *Journal of Metamorphic Geology*, *5*, 121–139. https://doi.org/10.1111/j.1525-1314.1987.tb00375.x

Parrish, R. R. (1992). U-Pb ages of Jurassic-Eocene plutonic rocks in the vicinity of the Valhalla Complex, southeastern British Columbia. In *Radiogenic age and isotopic studies: Report 5*. Geological Survey Canada Paper 91-2 (pp. 115–134). Geological Survey of Canada: Ottawa.

Pattison, D. R. M. (1989). P-T conditions and the influence of graphite on pelitic phase relations in the Ballachulish aureole, Scotland. *Journal of Petrology*, *30*, 1219–1244. https://doi.org/10.1093/petrology/30.5.1219

Pattison, D. R. M. (1992). Stability of andalusite and sillimanite and the Al_2SiO_5 triple point: Constraints from the Ballachulish aureole, Scotland. *Journal of Geology*, *100*, 423–446. https://doi.org/10.1086/629596

Pattison, D. R. M. (2006). The fate of graphite in prograde metamorphism of pelites: An example from the Ballachulish aureole, Scotland. *Lithos*, *88*, 85–99. https://doi.org/10.1016/j.lithos.2005.08.006

Pattison, D. R. M. (2013). Regional metamorphism in the Ballachulish area, SW Highlands, Scotland: New perspectives on a famous old debate, with regional implications. *Journal of the Geological Society of London*, *170*, 417–434. https://doi.org/10.1144/jgs2012-091

Pattison, D. R. M., de Capitani, C., & Gaidies, F. (2011). Petrologic consequences of variations in metamorphic reaction affinity. *Journal of Metamorphic Geology*, *29*, 953–977. https://doi.org/10.1111/j.1525-1314.2011.00950.x

Pattison, D. R. M., & DeBuhr, C. L. (2015). Petrology of metapelites in the Bugaboo aureole, British Columbia, Canada. *Journal of Metamorphic Geology*, *33*, 437–462. https://doi.org/10.1111/jmg.12128

Pattison, D., & Harte, B. (1985). A petrogenetic grid for pelites in the Ballachulish aureole and other Scottish thermal aureoles. *Journal of the Geological Society of London*, *142*, 7–28. https://doi.org/10.1144/gsjgs.142.1.0007

Pattison, D. R. M., & Harte, B. (1991). Petrography and mineral chemistry of pelites. In G. Voll, J. Töpel, D. R. M. Pattison & F. Seifert (Eds.), *Equilibrium and kinetics in contact metamorphism: The Ballachulish igneous complex and its thermal aureole* (pp. 135–180). Heidelberg, Germany: Springer Verlag. https://doi.org/10.1007/978-3-642-76145-4

Pattison, D. R. M., & Harte, B. (1997). The geology and evolution of the Ballachulish igneous complex and Aureole. *Scottish Journal of Geology*, *33*, 1–29. https://doi.org/10.1144/sjg33010001

Pattison, D. R. M., & Harte, B. (2001). *The Ballachulish igneous complex and aureole: A field guide*. Edinburgh, UK: Edinburgh Geological Society, 148 pp.

Pattison, D. R. M., Spear, F. S., BeBuhr, C. L., Cheney, J. T., & Guidotti, C. V. (2002). Thermodynamic modelling of the reaction Muscovite + Cordierite = Al_2SiO_5 + Biotite + Quartz + H_2O: Constraints from natural assemblages and implications for the metapelitic petrogenetic grid. *Journal of Metamorphic Geology*, *20*, 99–118. https://doi.org/10.1046/j.0263-4929.2001.356.356.x

Pattison, D. R. M., & Tinkham, D. T. (2009). Interplay between equilibrium and kinetics in prograde metamorphism of pelites: An example from the Nelson aureole, British Columbia. *Journal of Metamorphic Geology*, *27*, 249–279. https://doi.org/10.1111/j.1525-1314.2009.00816.x

Pattison, D. R. M., & Tracy, R. J. (1991). Phase equilibria and thermobarometry of metapelites. In D. M. Kerrick (Ed.), *Contact metamorphism*. *Mineralogical Society of America Reviews in Mineralogy*, *26*, 105–206.

Pattison, D. R. M., & Vogl, J. J. (2005). Contrasting sequences of metapelitic mineral-assemblages in the aureole of the tilted Nelson Batholith, British Columbia: Implications for phase equilibria and pressure determination in andalusite-sillimanite type settings. *Canadian Mineralogist*, *43*, 51–88. https://doi.org/10.2113/gscanmin.43.1.51

Pattison, D. R. M., & Voll, G. (1991). Regional geology of the Ballachulish area. In G. Voll, J. Töpel, D. R. M. Pattison & F. Seifert (Eds.), *Equilibrium and kinetics in contact metamorphism: The Ballachulish igneous complex and its thermal aureole* (pp. 19–38). Heidelberg, Germany: Springer Verlag. https://doi.org/10.1007/978-3-642-76145-4

Powell, W. G., & Ghent, E. D. (1996). Low-pressure metamorphism of the mafic volcanic rocks of the Rossland Group, southeastern British Columbia. *Canadian Journal of Earth Sciences*, *33*, 1402–1409. https://doi.org/10.1139/e96-105

Sevigny, J. H., & Parrish, R. R. (1993). Age and origin of Late Jurassic and Paleocene granitoids, Nelson Batholith, southern British Columbia. *Canadian Journal of Earth Sciences*, *30*, 2305–2314. https://doi.org/10.1139/e93-200

Spear, F. S., Thomas, J. B., & Hallett, B. W. (2014). Overstepping the garnet isograd: A comparison of QuiG barometry and thermodynamic modelling. *Contributions to Mineralogy and Petrology*, *168*, 1059. https://doi.org/10.1007/s00410-014-1059-6

Starr, P. G. (2017). *Sub-greenschist to lower amphibolite facies metamorphisk of basalts: Examples from Flin Flon, Manitoba and Rossland, British Columbia*. Unpublished PhD thesis, University of Calgary, 495 pp.

Tinkham, D. K., & Ghent, E. D. (2005). Estimating P-T conditions of garnet growth with isochemical phase diagram sections and the problem of effective bulk-composition. *Canadian Mineralogist*, *43*, 35–50. https://doi.org/10.2113/gscanmin.43.1.35

Tinkham, D. K., Zuluaga, C. A., & Stowell, H. H. (2001). Metapelite phase equilibria modelling in MnNCKFMASH: The effect of variable Al_2O_3 and MgO/(MgO+FeO) on mineral stability. *Mineralogical Society of America: Geological Materials Research*, *3*, 1–42.

Tomkins, H. S., & Pattison, D. R. M. (2007). Accessory phase petrogenesis in relation to major phase assemblages in pelites from the Nelson contact aureole, southern British Columbia. *Journal of Metamorphic Geology*, *25*, 401–421. https://doi.org/10.1111/j.1525-1314.2007.00702.x

Vogl, J. J., & Simony, P. S. (1992). The southern tail of the Nelson Batholith, southeast British Columbia: Structure and emplacement. *Geological Survey of Canada Paper*, *92-1A*, 71–76.

Voll, G., Töpel, J., Pattison, D. R. M., & Seifert, F. (Eds.) (1991). *Equilibrium and kinetics in contact metamorphism: The Ballachulish igneous complex and its aureole*. Heidelberg, Germany: Springer Verlag, 484 pp.

Wada, H., Tomita, T., Matsuura, K., Iuchi, K., Ito, M., & Morikiyo, T. (1994). Graphitization of carbonaceous matter during metamorphism with reference to carbonate and pelitic rocks of contact and regional metamorphisms, Japan. *Contributions to Mineralogy and Petrology*, *118*, 217–228. https://doi.org/10.1007/BF00306643

Weiss, S., & Troll, G. (1989). The Ballachulish Igneous Complex, Scotland: Petrography, mineral chemistry and order of crystallisation in the monzodiorite-quartz diorite suite and in the granite. *Journal of Petrology*, *30*, 1069–1116. https://doi.org/10.1093/petrology/30.5.1069

Weiss, S., & Troll, G. (1991). Thermal conditions and crystallisation sequence in the Ballachulish Complex. In G. Voll, J. Töpel, D. R. M. Pattison & F. Seifert (Eds.), *Equilibrium and kinetics in contact metamorphism: The Ballachulish igneous complex and its thermal aureole* (pp. 67–98). Heidelberg, Germany: Springer Verlag. https://doi.org/10.1007/978-3-642-76145-4

White, R. W., Pomroy, N. E., & Powell, R. (2005). An in-situ metatexite-diatexite transition in upper amphibolite facies rocks from Broken Hill, Australia. *Journal of Metamorphic Geology*, *23*, 579–602. https://doi.org/10.1111/j.1525-1314.2005.00597.x

White, R. W., Powell, R., & Holland, T. J. B. (2007). Progress relating to calculation of partial melting equilibria for metapelites.

Journal of Metamorphic Geology, *25*, 511–527. https://doi.org/10.1111/j.1525-1314.2007.00711.x

White, R. W., Powell, R., Holland, T. J. B., Johnson, T. E., & Green, C. R. (2014). New mineral activity–composition relations for thermodynamic calculations in metapelitic systems. *Journal of Metamorphic Geology*, *32*, 261–286. https://doi.org/10.1111/jmg.12071

White, R. W., Powell, R., & Johnson, T. E. (2014). The effect of Mn on mineral stability in metapelites revisited: New a-x relations for manganese-bearing minerals. *Journal of Metamorphic Geology*, *32*, 809–828. https://doi.org/10.1111/jmg.12095

Wiederkehr, M., Bousquet, R., Ziemann, M. A., Berger, A., & Schmid, S. M. (2011). 3-D assessment of peak-metamorphic conditions by Raman spectroscopy of carbonaceous material: An example from the margin of the Lepontine dome (Swiss Central Alps). *International Journal of Earth Sciences*, *100*, 1029–1063. https://doi.org/10.1007/s00531-010-0622-2

Wopenka, B., & Pasteris, J. D. (1993). Structural characterization of kerogens to granulite-facies graphite: Applicability of Raman microprobe spectroscopy. *American Mineralogist*, *78*, 533–557.

How to cite this article: Beyssac O, Pattison DRM, Bourdelle F. Contrasting degrees of recrystallization of carbonaceous material in the Nelson aureole, British Columbia and Ballachulish aureole, Scotland, with implications for thermometry based on Raman spectroscopy of carbonaceous material. *J Metamorph Geol*. 2018;00:1–25. https://doi.org/10.1111/jmg.12449